Monitoring Cointegrating Polynomial Regressions

Supplementary Appendix B: Local Asymptotic Power

Fabian Knorre, Martin Wagner and Maximilian Grupe

Local Asymptotic Power

In this appendix we consider local asymptotic power (LAP) in models of the form in (1) in the main document with the following specifications: Intercept and intercept plus linear trend, up to four integrated regressors and consecutive powers of up to order three of one of the integrated regressors. Denote as in the main text, w.l.o.g., x_{kt} as the I(1) regressor considered to enter the regression model with powers larger than one. The LAP results are based on 10,000 replications using time series of length 1,000 of i.i.d. standard normals to approximate the limiting distributions. The limiting distributions underlying LAP, as discussed in Proposition 3(b), are based on the functional central limit theorems for the scaled partial sum residual processes under the local alternatives discussed in Appendix A. In particular these FCLTs are given in:

- Local I(1) breaks ($\{u_t\}$ changes its behavior from I(0) to I(1)): Equation (47) in Appendix A.
- Local trend breaks: Equation (48) in Appendix A.
- Local slope breaks: Equation (49) in Appendix A.

For local I(1) breaks the limiting distribution depends, in addition to the break magnitude parameter δ, on the ratio of the long-run variance ω_γ^2 of the additional error component $\{\gamma_t\}$ and the conditional long-run variance $\omega_{u\cdot v}^2$.[1] We set this ratio to $\frac{\omega_\gamma^2}{\omega_{u\cdot v}^2} \coloneqq 1$. Similarly, the limiting distribution in case of local slope breaks depends on the long-run covariance matrix $\mathbf{\Omega}_{vv}$ of the regressors. We set $\mathbf{\Omega}_{vv} \coloneqq I_k$. The parameter δ determines the magnitude of a local I(1) break and

[1]Note: The limiting distribution underlying LAP in case of local I(1) breaks in Equation (30) of Wagner and Wied (2017) contains a typo. The long-run variance ω^2 must be replaced by the *conditional* long-run variance $\omega_{u\cdot v}^2$. This also holds for the corresponding discussion in the main text and in Supplementary Appendix B, where ω_ξ/ω must be replaced by $\omega_\xi/\omega_{u\cdot v}$.

varies in 1001 equidistant steps over the interval $[0, 10000]$. The value $\delta = 0$ corresponds to the null hypothesis. Similarly, Δ_{θ_D} indicates the magnitude of a local break in the coefficient of the linear trend.[2] The parameter Δ_{θ_D} varies in 751 equidistant steps over the interval $[0, 1500]$, with $\Delta_{\theta_D} = 0$ corresponding to the null hypothesis. In case of local slope breaks, the magnitude of a local break in the slope parameter is given by Δ_{θ_X}.[3] We consider 1001 equally spaced values of Δ_{θ_X} in the interval $[0, 10000]$, with $\Delta_{\theta_X} = 0$ corresponding to the null hypothesis. For local slope breaks we consider a local break either in the coefficient corresponding to x_{kt} or in the coefficient corresponding to x_{kt}^2. All simulations are performed at the 5% significance level.

With respect to the stochastic regressors, LAP depends upon k, the number of I(1) regressors, and p_k, the highest power of x_{kt}. Figure 1 displays for different values of k and p_k LAP against local I(1) breaks in the intercept and linear trend case using $\hat{H}^m$. As expected, LAP decreases when further I(1) regressors or higher powers are included. With this observation in mind, for the sake of brevity all other LAP results are presented only for the case including a single I(1) regressor and its square (i. e. , $k = 1$ and $p_k = 2$), considering both deterministic specifications, intercept and intercept and linear trend. This case also covers the quadratic EKC model, which we use in addition to the linear and cubic model in the empirical application in Section 4 in the main document.

In most considered settings the two detectors $\hat{H}^m$ and $\hat{H}_d^m$ lead to nearly identical LAP. In a few cases, however, LAP of $\hat{H}_d^m$ is considerably lower than that of $\hat{H}^m$. Therefore, we neglect $\hat{H}_d^m$ in our LAP analysis and focus on $\hat{H}^m$, $\hat{H}_{sn}^m$, $\hat{H}_{mov}^{m,n}$ and $\hat{H}_{mov,sn}^{m,n}$, for $n = 0.1, 0.2, 0.3$.

We start with local I(1) breaks and compare LAP with respect to the estimation method. Figure 2 displays LAP against local I(1) breaks in the intercept only case for FM-/D-OLS and IM-OLS using the four detectors $\hat{H}^m$, $\hat{H}_{sn}^m$, $\hat{H}_{mov}^{m,0.1}$ and $\hat{H}_{mov,sn}^{m,0.1}$. Calibration and break fraction are set to $m = 0.5$ and $r = 0.75$, respectively. For each of the four detectors FM-/D-OLS leads to higher LAP than IM-OLS. This result is independent of the choice of the window size, deterministic specification, calibration and break fraction and is in line with standard asymptotic theory concerning estimator efficiency. The next aspect considered is the impact of the window size on LAP and in addition the comparison to a detector without moving window. Figure 3 displays LAP against local I(1) breaks in

[2] In Proposition 3(b) Δ_{θ_D} refers to a vector defining changes of all elements of $\theta_D \in \mathbb{R}^q$, with $\Delta_{\theta_D} \in \mathbb{R}^q$. In the LAP analysis only a single element of θ_D changes. To avoid overloaded notation, Δ_{θ_D} denotes in the LAP analysis only the change in a single element, thus $\Delta_{\theta_D} \in \mathbb{R}$.

[3] The parameter Δ_{θ_X} refers in the LAP analysis – in a similar fashion as Δ_{θ_D} – to a scalar value, in contrast to Proposition 3(b) where $\Delta_{\theta_X} \in \mathbb{R}^p$.

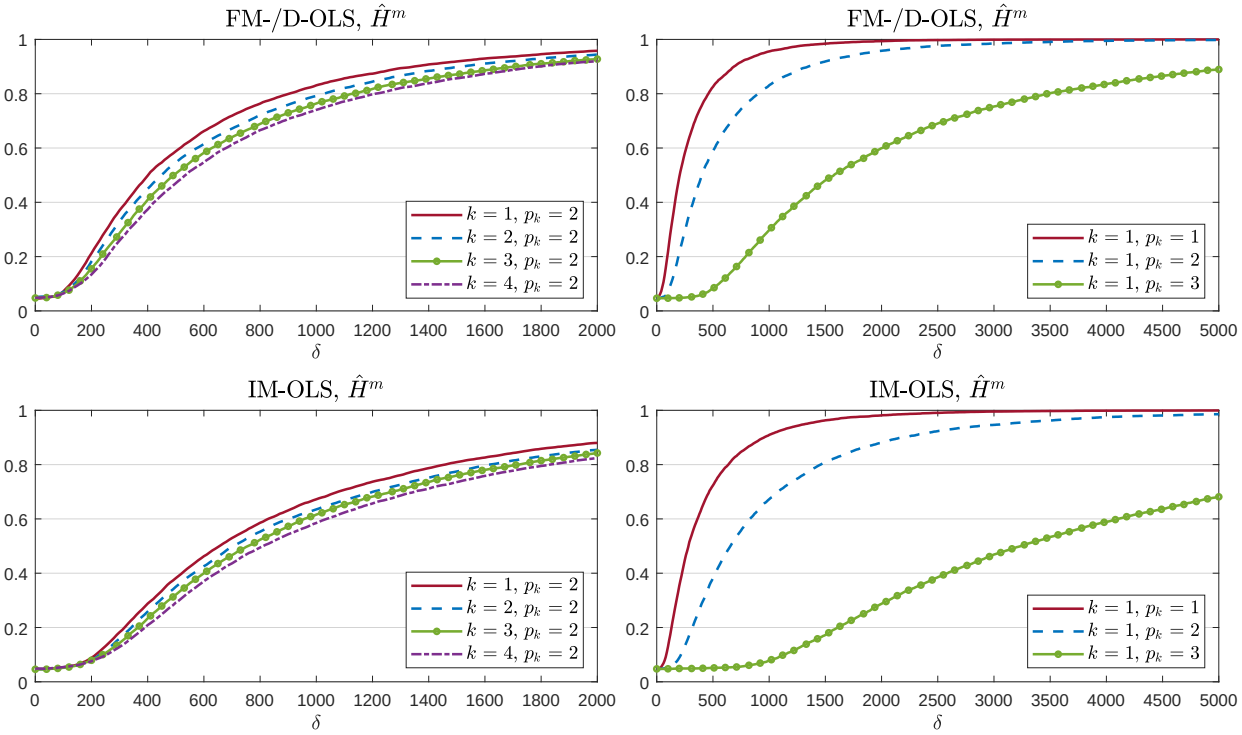

Figure 1: Local asymptotic power against I(1) breaks in the intercept and linear trend case for $\hat{H}^m$. The upper two plots correspond to FM-/D-OLS and the lower plots to IM-OLS. Calibration and break fraction are set to $m = 0.5$ and $r = 0.75$, respectively.

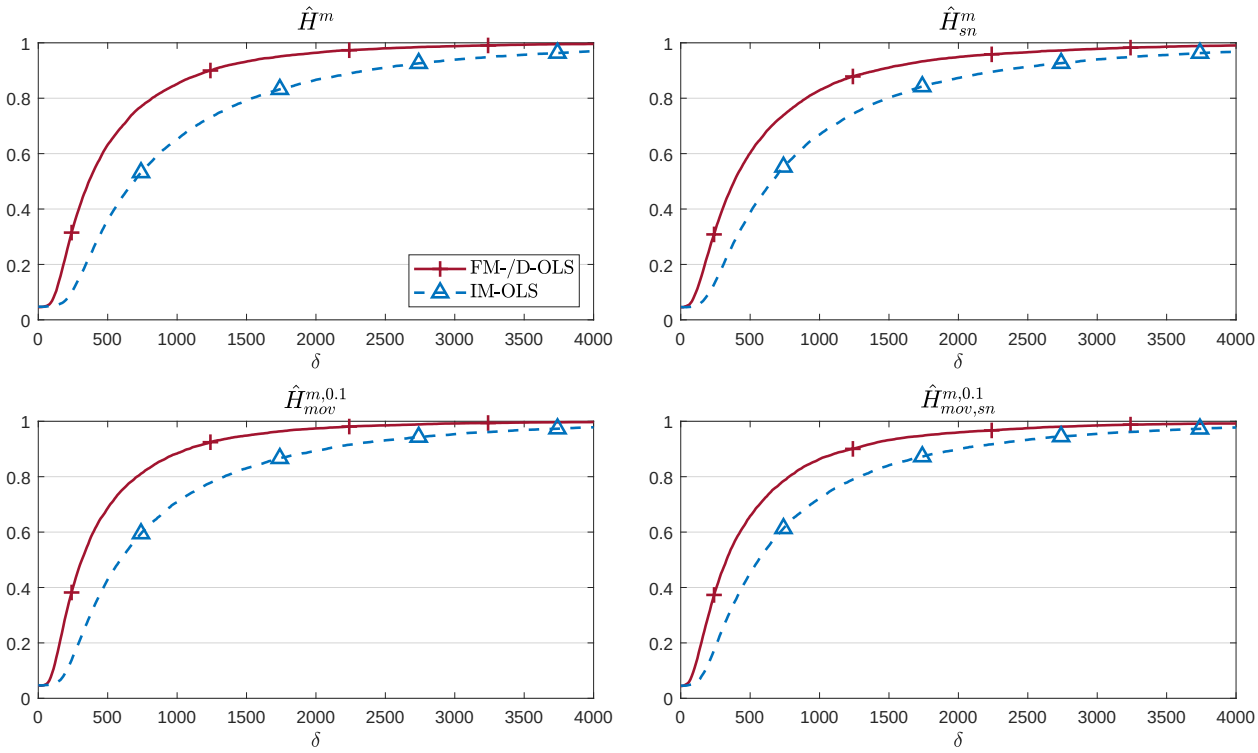

Figure 2: Local asymptotic power against I(1) breaks in the intercept only case for FM-/D-OLS and IM-OLS using $\hat{H}^m$, $\hat{H}^m_{sn}$, $\hat{H}^{m,0.1}_{mov}$ and $\hat{H}^{m,0.1}_{mov,sn}$. Calibration and break fraction are set to $m = 0.5$ and $r = 0.75$, respectively.

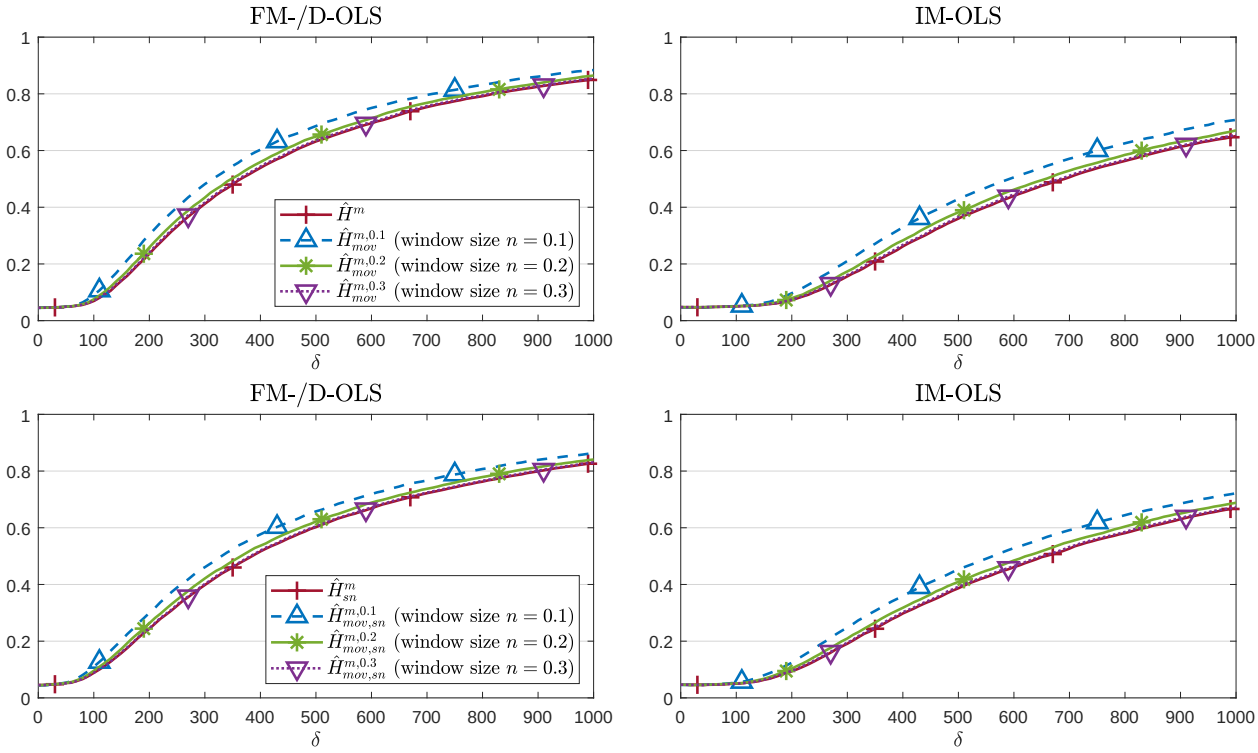

Figure 3: Local asymptotic power against I(1) breaks in the intercept only case for $\hat{H}^m$, $\hat{H}^m_{sn}$, $\hat{H}^{m,n}_{mov}$ and $\hat{H}^{m,n}_{mov,sn}$, for $n = 0.1, 0.2, 0.3$. The upper two plots correspond to standardized detectors, the lower two plots correspond to self-normalized detectors. Calibration and break fraction are set to $m = 0.5$ and $r = 0.75$, respectively.

the intercept only case for $\hat{H}^m$ and $\hat{H}^{m,n}_{mov}$, and their corresponding self-normalized counterparts $\hat{H}^m_{sn}$ and $\hat{H}^{m,n}_{mov,sn}$, for $n = 0.1, 0.2, 0.3$. Calibration and break fraction are set to $m = 0.5$ and $r = 0.75$, respectively. LAP is highest for the smallest window size $n = 0.1$, decreases with increasing window size and is lowest for the detector without moving window. This result is independent of estimator choice, self-normalization and also the choices of calibration and break fraction. However, the differences in LAP between the detectors are sometimes very small. Including a linear trend in the model does not cause any qualitative changes in the above results. The last aspect we consider for LAP against local I(1) breaks is the impact of self-normalization in comparison to standardization. Figure 4 shows the results for $\hat{H}^m_{sn}$ and $\hat{H}^{m,0.1}_{mov,sn}$, each compared to its standardized counterpart $\hat{H}^m$ and $\hat{H}^{m,0.1}_{mov}$, respectively, in case of local I(1) breaks with intercept only. Calibration and break fraction are set to $m = 0.5$ and $r = 0.75$. Self-normalization by and large reduces LAP for FM-/D-OLS and increases LAP for IM-OLS. Figure 5 displays the corresponding results if additionally a linear trend is included in the model. In this case, when using IM-OLS the advantage of self-

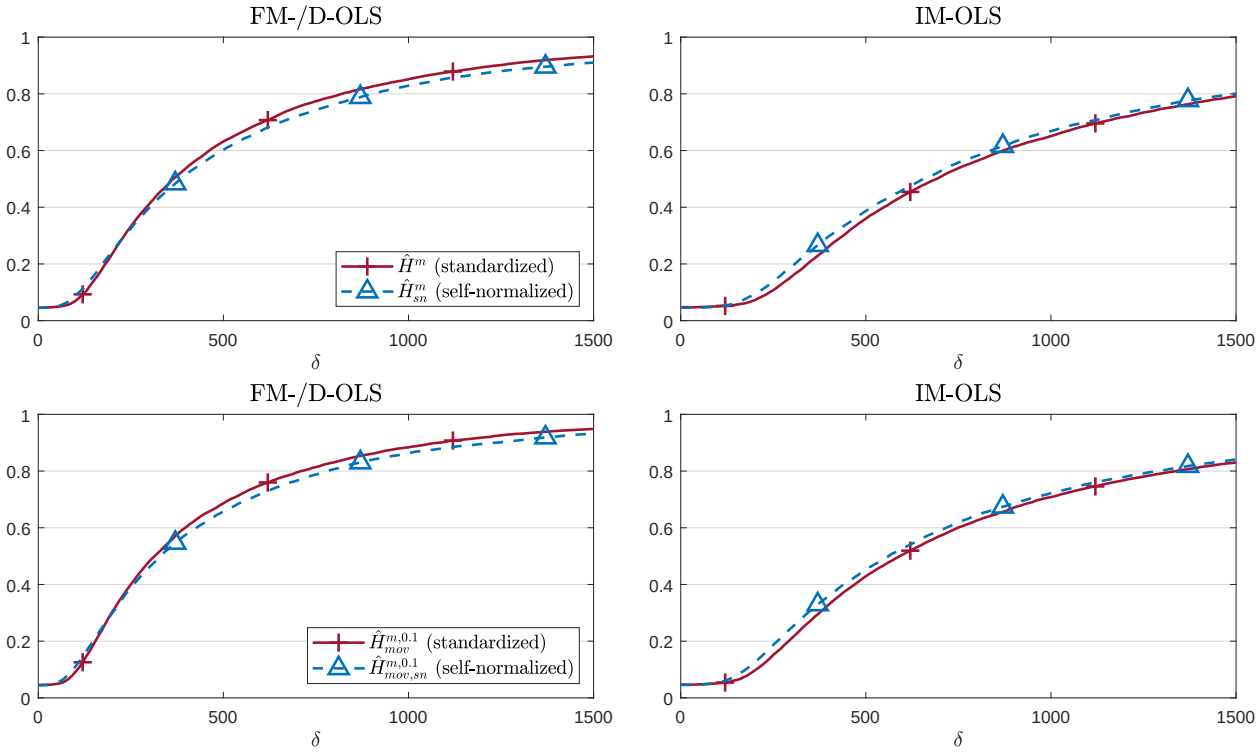

Figure 4: Local asymptotic power against local I(1) breaks in the intercept only case. The upper two plots correspond to $\hat{H}^m$ and $\hat{H}^m_{sn}$. The lower two plots correspond to $\hat{H}^{m,0.1}_{mov}$ and $\hat{H}^{m,0.1}_{mov,sn}$. Calibration and break fraction are set to $m = 0.5$ and $r = 0.75$, respectively.

normalization over standardization disappears. Changes in the window size or calibration and break fraction have no qualitative influence on the differences in LAP between standardized and self-normalized detectors.

We now turn briefly to LAP against local slope breaks. The results are qualitatively the same as in case of local I(1) breaks with respect to the estimation method, self-normalization, window size and deterministic specification and are independent of the calibration and break fraction. Corresponding LAP figures are available upon request.

Finally, we consider LAP in case of local trend breaks. The overall results are very similar to both cases, local I(1) and local slope breaks, but with two major differences: The first difference is that now calibration and break fraction influence which detector leads to the highest LAP. Figure 6 displays LAP for standardized detectors for $m = 0.5$ and $r \in \{0.5, 0.75\}$, with either $\hat{H}^m$ or $\hat{H}^{m,0.1}_{mov}$ leading to the highest LAP, depending on the choice of m and r. We obtain similar results for self-normalized detectors, with either $\hat{H}^m_{sn}$ or $\hat{H}^{m,0.1}_{mov,sn}$ leading to the highest LAP. The second difference in case of local trend breaks is the impact of self-normalization compared to standardization on

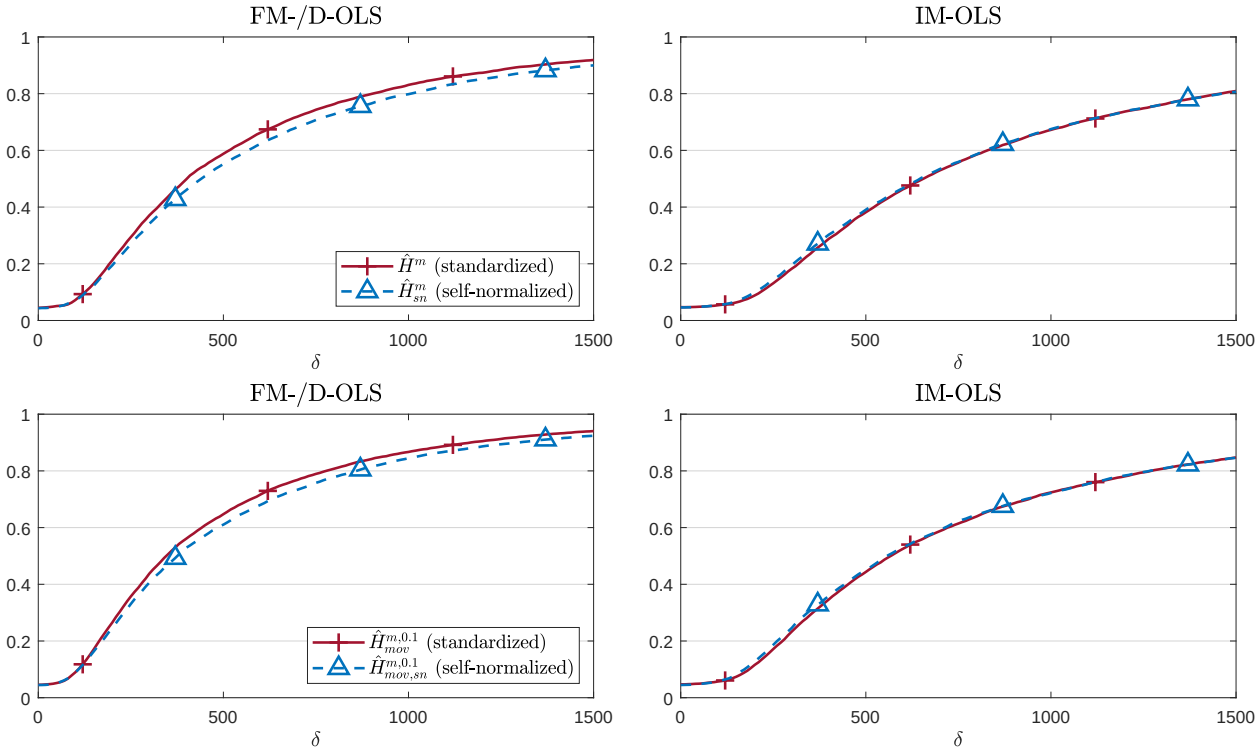

Figure 5: Local asymptotic power against local I(1) breaks in the intercept and linear trend case. For further explanations see notes for Figure 4.

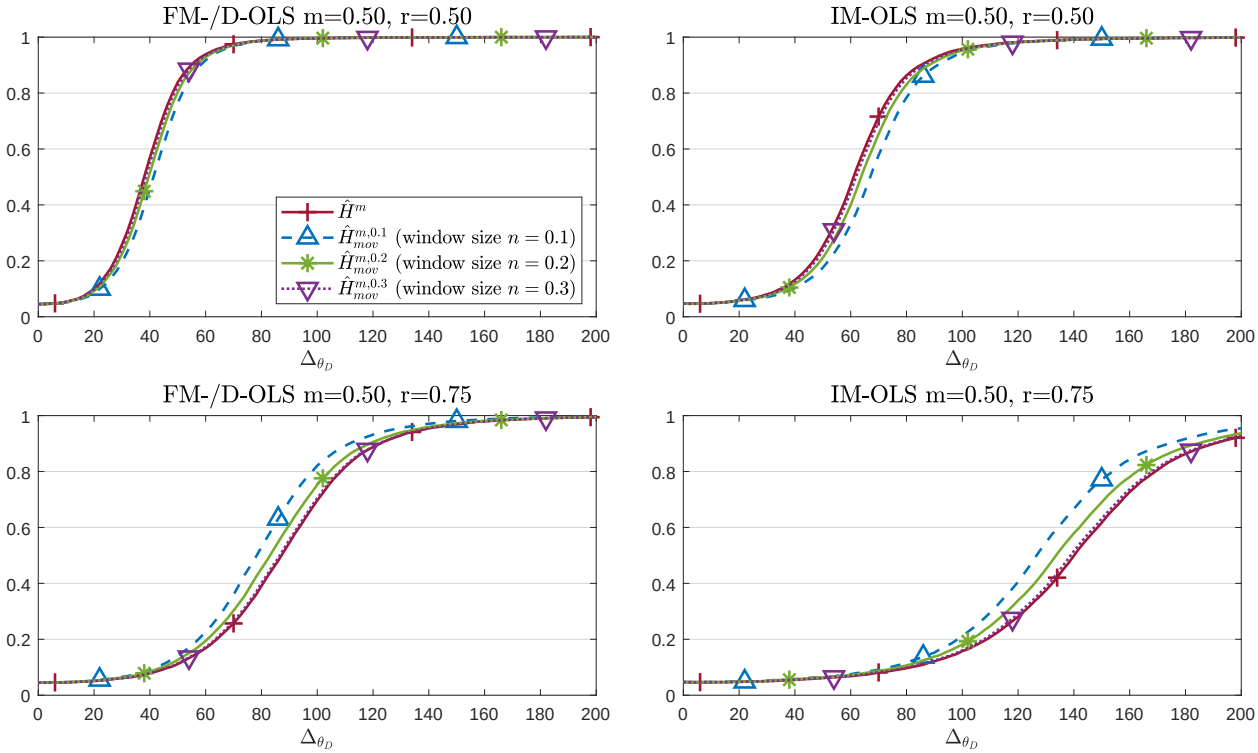

Figure 6: Local asymptotic power against local trend breaks for $\hat{H}^m$ and $\hat{H}^{m,n}_{mov}$ in the intercept and linear trend case. The upper two plots correspond to $m = r = 0.5$. The lower two plots correspond to $m = 0.5$ and $r = 0.75$.

LAP for IM-OLS. Figure 7 displays LAP in case of local trend breaks for $\hat{H}^m$, $\hat{H}^m_{sn}$, $\hat{H}^{m,0.1}_{mov}$ and $\hat{H}^{m,0.1}_{mov,sn}$, with $m = 0.5$ and $r = 0.75$. For IM-OLS, the two self-normalized detectors, each compared to its standardized counterpart, lead to higher LAP at smaller break magnitudes at the expense of lower LAP at larger break magnitudes. In contrast, in case of local I(1) or local slope breaks, self-normalization either leads to higher or nearly the same LAP as standardization for IM-OLS, regardless of the break magnitude. For FM-/D-OLS, standardization still leads to higher LAP than self-normalization, as is the case with local I(1) or local slope breaks.

In conclusion, the LAP results can be summarized as follows: First, given a certain detector, break type, calibration and break fraction, LAP is higher for FM-/D-OLS than for IM-OLS. This stems from the fact that for the linear case FM-/D-OLS is asymptotically conditionally more efficient than IM-OLS from a standard asymptotic theory point of view (see Vogelsang and Wagner, 2014a, Proposition 2). A similar result can be obtained for the CPR case. Second, moving window detectors with $n = 0.1$ are the best choice in case of local I(1) and local slope breaks. In case of local trend breaks there is no clear ranking. Third, self-normalization by and large reduces LAP for

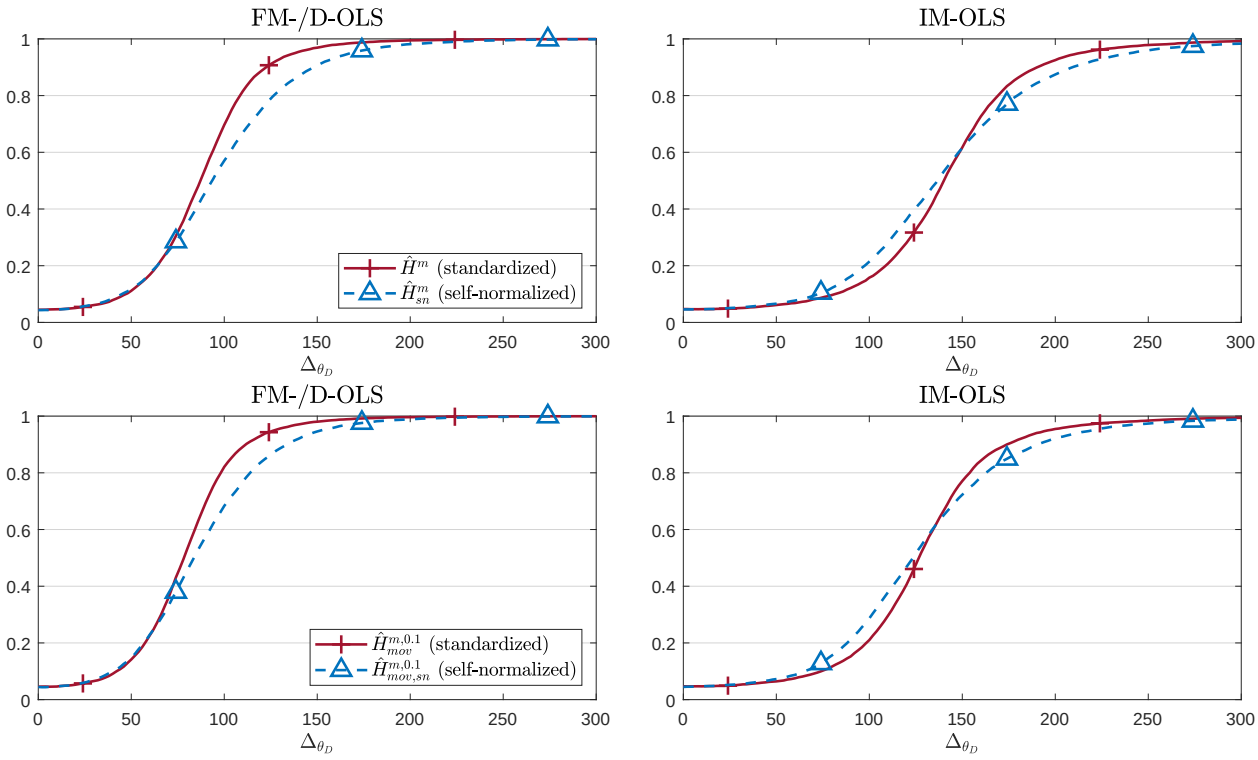

Figure 7: Local asymptotic power against local trend breaks in the model with intercept and linear trend. The upper two plots correspond to $\hat{H}^m$ and $\hat{H}^m_{sn}$. The lower two plots correspond to $\hat{H}^{m,0.1}_{mov}$ and $\hat{H}^{m,0.1}_{mov,sn}$. Calibration and break fraction are set to $m = 0.5$ and $r = 0.75$, respectively.

FM-/D-OLS. In contrast, for IM-OLS self-normalization is by and large advantageous, in case of local trend breaks at least for small break magnitudes. Fourth, local slope breaks lead, as expected, to almost identical LAP patterns as local I(1) breaks. Wagner and Wied (2017, p. 967) explain for the cointegrating linear regression model that the asymptotic behavior in case of slope breaks is similar to the case of I(1) breaks. The same holds for the CPR model when there is only a (local) break in the coefficient corresponding to one I(1) regressor: The slope coefficient after the break, $\theta_{X,1}$, can be separated into θ_X and $\theta_{X,1} - \theta_X$. The additional post break term $X_t'(\theta_{X,1} - \theta_X)$ is an I(1) process – since the coefficient corresponding to one I(1) regressors changes – and thus leads to similar asymptotic behavior as in case of local I(1) breaks, where $\{u_t\}$ changes its behavior from I(0) to I(1). Fifth, $\hat{H}^m$ is preferable to $\hat{H}_d^m$, since $\hat{H}^m$ performs either better or at least as good as $\hat{H}_d^m$ in all considered cases. Finally, regardless of the choice of estimation method and detector, the LAP results suggest to choose the calibration fraction m as large as possible.

The LAP analysis reveals indications about the behavior of the monitoring procedures in finite samples. In fact, we find by and large very similar relative performance results in the finite sample simulations in Section 3 in the main document as in the LAP analysis.

Monitoring Cointegrating Polynomial Regressions

Supplementary Appendix C: Additional Finite Sample Performance Results

Fabian Knorre, Martin Wagner and Maximilian Grupe

Finite Sample Performance

Null Rejection Probabilities

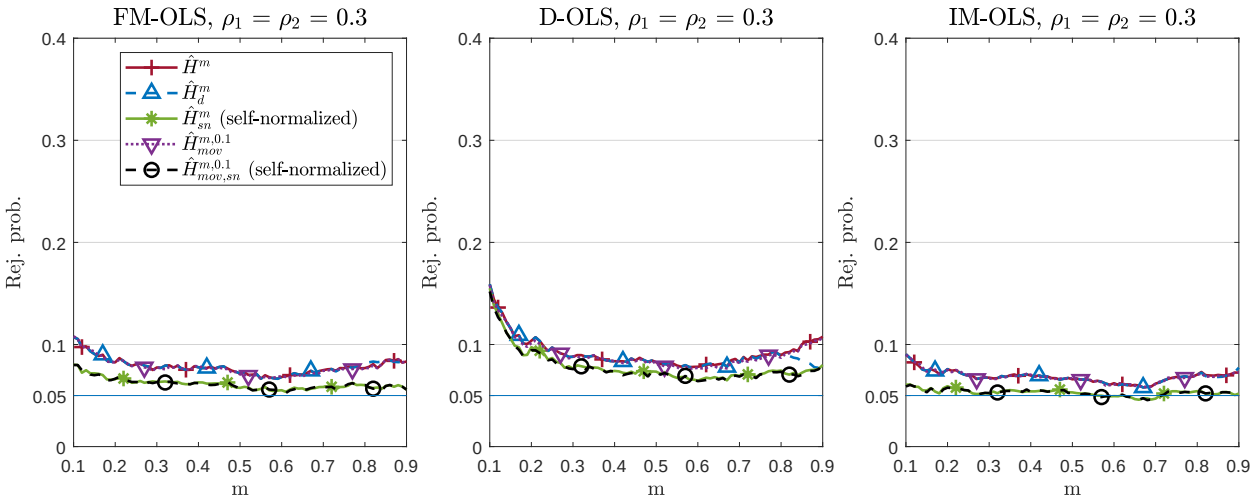

Figure 8: Empirical null rejection probabilities for a grid of values of m, with $T = 500$ and $\rho_1 = \rho_2 = 0.3$.

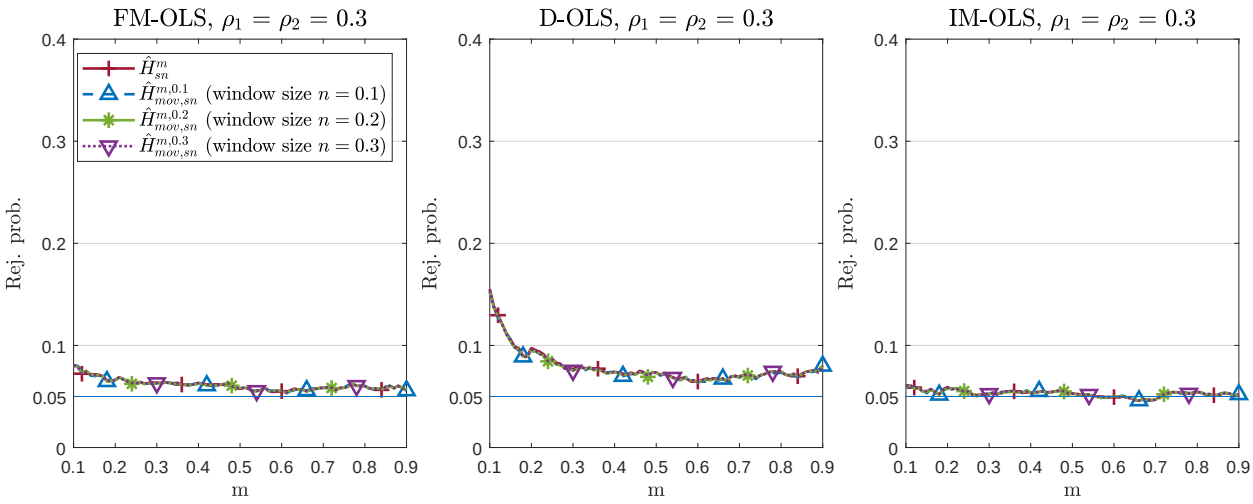

Figure 9: Empirical null rejection probabilities for a grid of values of m, with $T = 500$ and $\rho_1 = \rho_2 = 0.3$.

Size-Corrected Power – I(1) Breaks

In addition to Section 3 in the main document, Tables 1 to 6 display size-corrected power results in case of I(1) breaks for $\rho_1 = \rho_2 \in \{0, 0.6, 0.9\}$ with $T \in \{200, 500\}$. The findings are similar as for $\rho_1 = \rho_2 = 0.3$ in the main text: Size-corrected power is by and large highest for $\hat{H}^{m,0.1}_{mov}$ or $\hat{H}^{m,0.1}_{mov,sn}$ and lower for IM-OLS than for FM-OLS and D-OLS.

$\rho_1 = \rho_2 = 0.0$			$m = 0.25$			$m = 0.5$			$m = 0.75$		
		r	0.25	0.5	0.75	0.25	0.5	0.75	0.25	0.5	0.75
$\hat{H}^m$	FM		0.26	0.08	0.05	0.37	0.76	0.21	0.38	0.51	0.87
	D		0.19	0.06	0.05	0.37	0.71	0.17	0.39	0.51	0.85
	IM		0.15	0.06	0.05	0.32	0.61	0.11	0.38	0.47	0.77
$\hat{H}^m_d$	FM		0.26	0.08	0.05	0.37	0.76	0.21	0.37	0.50	0.87
	D		0.19	0.06	0.05	0.37	0.71	0.17	0.39	0.51	0.85
	IM		0.15	0.06	0.05	0.32	0.61	0.11	0.38	0.47	0.77
$\hat{H}^m_{sn}$	FM		0.28	0.08	0.05	0.18	0.73	0.21	0.17	0.27	0.85
	D		0.20	0.07	0.05	0.23	0.69	0.17	0.22	0.33	0.83
	IM		0.18	0.06	0.05	0.22	0.62	0.12	0.23	0.34	0.77
$\hat{H}^{m,0.1}_{mov}$	FM		0.26	0.07	0.05	0.37	0.77	0.26	0.38	0.51	0.87
	D		0.18	0.06	0.05	0.36	0.73	0.22	0.39	0.51	0.85
	IM		0.14	0.06	0.05	0.32	0.63	0.14	0.37	0.46	0.78
$\hat{H}^{m,0.2}_{mov}$	FM		0.26	0.08	0.05	0.37	0.76	0.23	0.38	0.51	0.87
	D		0.18	0.07	0.05	0.36	0.72	0.19	0.39	0.51	0.85
	IM		0.15	0.06	0.05	0.32	0.62	0.12	0.38	0.47	0.77
$\hat{H}^{m,0.3}_{mov}$	FM		0.26	0.08	0.05	0.37	0.75	0.21	0.38	0.51	0.87
	D		0.18	0.06	0.05	0.36	0.71	0.17	0.39	0.51	0.85
	IM		0.15	0.06	0.05	0.32	0.61	0.11	0.38	0.47	0.77
$\hat{H}^{m,0.1}_{mov,sn}$	FM		0.29	0.08	0.05	0.18	0.75	0.26	0.17	0.28	0.86
	D		0.21	0.07	0.05	0.23	0.71	0.21	0.22	0.33	0.84
	IM		0.17	0.06	0.05	0.21	0.63	0.15	0.22	0.33	0.77
$\hat{H}^{m,0.2}_{mov,sn}$	FM		0.29	0.08	0.05	0.18	0.74	0.23	0.17	0.27	0.85
	D		0.21	0.07	0.05	0.23	0.69	0.18	0.22	0.33	0.83
	IM		0.17	0.06	0.05	0.22	0.63	0.14	0.23	0.34	0.76
$\hat{H}^{m,0.3}_{mov,sn}$	FM		0.29	0.08	0.05	0.18	0.73	0.22	0.17	0.27	0.85
	D		0.21	0.07	0.05	0.23	0.69	0.17	0.22	0.33	0.83
	IM		0.17	0.06	0.05	0.22	0.62	0.13	0.23	0.34	0.77

Table 1: Size-corrected power against $I(1)$ breaks for $T = 200$ and $\rho_1 = \rho_2 = 0.0$.

$\rho_1 = \rho_2 = 0.6$			$m = 0.25$			$m = 0.5$			$m = 0.75$		
		r	0.25	0.5	0.75	0.25	0.5	0.75	0.25	0.5	0.75
$\hat{H}^m$	FM		0.11	0.06	0.05	0.24	0.44	0.08	0.27	0.36	0.64
	D		0.09	0.05	0.05	0.23	0.40	0.07	0.29	0.38	0.61
	IM		0.07	0.05	0.05	0.19	0.27	0.06	0.26	0.32	0.48
$\hat{H}_d^m$	FM		0.11	0.06	0.05	0.24	0.44	0.08	0.27	0.36	0.64
	D		0.09	0.05	0.05	0.23	0.40	0.07	0.28	0.37	0.61
	IM		0.07	0.05	0.05	0.19	0.27	0.06	0.26	0.32	0.48
$\hat{H}_{sn}^m$	FM		0.12	0.06	0.05	0.15	0.42	0.08	0.14	0.23	0.62
	D		0.10	0.06	0.05	0.17	0.38	0.07	0.17	0.25	0.58
	IM		0.07	0.05	0.05	0.15	0.29	0.06	0.18	0.27	0.48
$\hat{H}_{mov}^{m,0.1}$	FM		0.10	0.06	0.05	0.23	0.45	0.09	0.27	0.36	0.64
	D		0.09	0.05	0.05	0.22	0.41	0.08	0.29	0.38	0.62
	IM		0.06	0.05	0.05	0.18	0.26	0.06	0.25	0.31	0.48
$\hat{H}_{mov}^{m,0.2}$	FM		0.10	0.06	0.05	0.24	0.45	0.08	0.27	0.36	0.64
	D		0.09	0.05	0.05	0.22	0.40	0.07	0.29	0.38	0.61
	IM		0.07	0.05	0.05	0.19	0.27	0.06	0.26	0.32	0.48
$\hat{H}_{mov}^{m,0.3}$	FM		0.11	0.06	0.05	0.24	0.44	0.08	0.27	0.36	0.64
	D		0.09	0.05	0.05	0.22	0.40	0.07	0.29	0.38	0.61
	IM		0.07	0.05	0.05	0.19	0.27	0.06	0.26	0.32	0.48
$\hat{H}_{mov,sn}^{m,0.1}$	FM		0.12	0.06	0.05	0.15	0.43	0.10	0.15	0.23	0.62
	D		0.10	0.06	0.05	0.17	0.39	0.08	0.17	0.25	0.59
	IM		0.07	0.05	0.05	0.14	0.27	0.06	0.18	0.26	0.49
$\hat{H}_{mov,sn}^{m,0.2}$	FM		0.12	0.06	0.05	0.15	0.42	0.09	0.14	0.23	0.62
	D		0.09	0.06	0.05	0.17	0.38	0.08	0.17	0.25	0.58
	IM		0.07	0.05	0.05	0.15	0.28	0.06	0.18	0.26	0.48
$\hat{H}_{mov,sn}^{m,0.3}$	FM		0.12	0.06	0.05	0.15	0.42	0.08	0.14	0.23	0.62
	D		0.09	0.06	0.05	0.17	0.38	0.07	0.17	0.25	0.58
	IM		0.07	0.05	0.05	0.15	0.28	0.06	0.18	0.27	0.48

Table 2: Size-corrected power against $I(1)$ breaks for $T = 200$ and $\rho_1 = \rho_2 = 0.6$.

$\rho_1 = \rho_2 = 0.9$			$m = 0.25$			$m = 0.5$			$m = 0.75$		
		r	0.25	0.5	0.75	0.25	0.5	0.75	0.25	0.5	0.75
$\hat{H}^m$	FM		0.06	0.05	0.05	0.10	0.10	0.05	0.13	0.13	0.17
	D		0.06	0.05	0.05	0.10	0.10	0.06	0.14	0.15	0.16
	IM		0.05	0.05	0.05	0.08	0.06	0.05	0.12	0.12	0.11
$\hat{H}_d^m$	FM		0.06	0.05	0.05	0.10	0.10	0.05	0.13	0.13	0.17
	D		0.06	0.05	0.05	0.10	0.10	0.06	0.14	0.15	0.16
	IM		0.05	0.05	0.05	0.08	0.06	0.05	0.12	0.12	0.11
$\hat{H}_{sn}^m$	FM		0.06	0.05	0.05	0.08	0.09	0.05	0.08	0.10	0.15
	D		0.06	0.05	0.05	0.08	0.10	0.05	0.10	0.11	0.15
	IM		0.05	0.05	0.05	0.07	0.07	0.05	0.11	0.11	0.12
$\hat{H}_{mov}^{m,0.1}$	FM		0.06	0.05	0.05	0.09	0.09	0.05	0.13	0.13	0.17
	D		0.06	0.05	0.05	0.10	0.10	0.06	0.14	0.15	0.16
	IM		0.05	0.05	0.05	0.08	0.06	0.05	0.12	0.12	0.11
$\hat{H}_{mov}^{m,0.2}$	FM		0.06	0.05	0.05	0.10	0.10	0.05	0.13	0.13	0.17
	D		0.06	0.05	0.05	0.10	0.10	0.06	0.14	0.15	0.16
	IM		0.05	0.05	0.05	0.08	0.06	0.05	0.12	0.12	0.11
$\hat{H}_{mov}^{m,0.3}$	FM		0.06	0.05	0.05	0.10	0.10	0.05	0.13	0.13	0.17
	D		0.06	0.05	0.05	0.10	0.10	0.05	0.14	0.15	0.16
	IM		0.05	0.05	0.05	0.08	0.06	0.05	0.12	0.12	0.11
$\hat{H}_{mov,sn}^{m,0.1}$	FM		0.06	0.05	0.05	0.08	0.10	0.06	0.09	0.10	0.15
	D		0.06	0.05	0.05	0.09	0.10	0.06	0.10	0.11	0.15
	IM		0.05	0.05	0.05	0.07	0.07	0.05	0.11	0.11	0.12
$\hat{H}_{mov,sn}^{m,0.2}$	FM		0.06	0.05	0.05	0.08	0.09	0.05	0.08	0.10	0.15
	D		0.06	0.05	0.05	0.09	0.10	0.06	0.10	0.11	0.15
	IM		0.05	0.05	0.05	0.07	0.07	0.05	0.11	0.11	0.12
$\hat{H}_{mov,sn}^{m,0.3}$	FM		0.06	0.05	0.05	0.08	0.09	0.05	0.08	0.10	0.15
	D		0.06	0.05	0.05	0.08	0.10	0.05	0.10	0.11	0.15
	IM		0.05	0.05	0.05	0.07	0.07	0.05	0.11	0.11	0.12

Table 3: Size-corrected power against $I(1)$ breaks for $T = 200$ and $\rho_1 = \rho_2 = 0.9$.

$\rho_1 = \rho_2 = 0.0$			$m = 0.25$			$m = 0.5$			$m = 0.75$		
		r	0.25	0.5	0.75	0.25	0.5	0.75	0.25	0.5	0.75
$\hat{H}^m$	FM		0.78	0.36	0.06	0.48	0.97	0.59	0.49	0.61	0.99
	D		0.75	0.33	0.06	0.47	0.96	0.56	0.50	0.62	0.98
	IM		0.58	0.19	0.05	0.38	0.89	0.38	0.48	0.57	0.95
$\hat{H}_d^m$	FM		0.78	0.36	0.06	0.48	0.97	0.59	0.51	0.65	0.99
	D		0.75	0.33	0.06	0.47	0.96	0.56	0.50	0.62	0.98
	IM		0.58	0.19	0.05	0.38	0.89	0.38	0.47	0.57	0.95
$\hat{H}_{sn}^m$	FM		0.76	0.36	0.06	0.21	0.95	0.57	0.18	0.31	0.98
	D		0.74	0.32	0.06	0.23	0.95	0.54	0.21	0.34	0.98
	IM		0.60	0.20	0.05	0.24	0.90	0.41	0.25	0.38	0.95
$\hat{H}_{mov}^{m,0.1}$	FM		0.82	0.38	0.07	0.49	0.98	0.65	0.49	0.61	0.99
	D		0.79	0.34	0.07	0.48	0.97	0.62	0.50	0.62	0.98
	IM		0.61	0.18	0.06	0.38	0.92	0.45	0.47	0.57	0.96
$\hat{H}_{mov}^{m,0.2}$	FM		0.80	0.37	0.06	0.48	0.97	0.61	0.49	0.61	0.99
	D		0.77	0.34	0.06	0.47	0.96	0.58	0.50	0.62	0.98
	IM		0.60	0.19	0.05	0.38	0.90	0.40	0.47	0.57	0.95
$\hat{H}_{mov}^{m,0.3}$	FM		0.79	0.37	0.06	0.48	0.97	0.59	0.49	0.61	0.99
	D		0.76	0.33	0.06	0.47	0.96	0.57	0.50	0.62	0.98
	IM		0.58	0.19	0.05	0.38	0.89	0.38	0.48	0.57	0.95
$\hat{H}_{mov,sn}^{m,0.1}$	FM		0.80	0.38	0.07	0.21	0.96	0.63	0.19	0.31	0.98
	D		0.78	0.34	0.07	0.22	0.96	0.59	0.21	0.33	0.98
	IM		0.63	0.20	0.05	0.23	0.92	0.47	0.25	0.38	0.96
$\hat{H}_{mov,sn}^{m,0.2}$	FM		0.77	0.37	0.07	0.21	0.96	0.59	0.18	0.31	0.98
	D		0.76	0.33	0.06	0.22	0.95	0.56	0.21	0.34	0.98
	IM		0.61	0.21	0.05	0.23	0.90	0.43	0.25	0.38	0.95
$\hat{H}_{mov,sn}^{m,0.3}$	FM		0.76	0.36	0.06	0.21	0.95	0.58	0.18	0.31	0.98
	D		0.74	0.33	0.06	0.23	0.95	0.55	0.21	0.34	0.98
	IM		0.60	0.20	0.05	0.24	0.90	0.41	0.25	0.38	0.95

Table 4: Size-corrected power against $I(1)$ breaks for $T = 500$ and $\rho_1 = \rho_2 = 0.0$.

$\rho_1 = \rho_2 = 0.6$			$m = 0.25$			$m = 0.5$			$m = 0.75$		
		r	0.25	0.5	0.75	0.25	0.5	0.75	0.25	0.5	0.75
$\hat{H}^m$	FM		0.44	0.13	0.05	0.40	0.82	0.27	0.42	0.53	0.91
	D		0.40	0.11	0.05	0.38	0.80	0.24	0.43	0.54	0.89
	IM		0.21	0.07	0.05	0.31	0.66	0.13	0.40	0.49	0.80
$\hat{H}_d^m$	FM		0.44	0.13	0.05	0.40	0.82	0.27	0.41	0.53	0.90
	D		0.40	0.11	0.05	0.38	0.80	0.24	0.41	0.53	0.89
	IM		0.21	0.07	0.05	0.31	0.66	0.13	0.40	0.49	0.80
$\hat{H}_{sn}^m$	FM		0.43	0.13	0.05	0.19	0.79	0.26	0.17	0.28	0.88
	D		0.39	0.12	0.05	0.20	0.78	0.24	0.18	0.29	0.87
	IM		0.23	0.07	0.05	0.21	0.67	0.15	0.23	0.34	0.79
$\hat{H}_{mov}^{m,0.1}$	FM		0.46	0.13	0.05	0.40	0.85	0.34	0.42	0.53	0.91
	D		0.42	0.11	0.05	0.38	0.83	0.30	0.43	0.54	0.90
	IM		0.21	0.07	0.05	0.30	0.67	0.16	0.40	0.48	0.81
$\hat{H}_{mov}^{m,0.2}$	FM		0.45	0.13	0.05	0.40	0.83	0.29	0.42	0.53	0.90
	D		0.42	0.12	0.05	0.38	0.81	0.26	0.43	0.54	0.89
	IM		0.21	0.07	0.05	0.30	0.66	0.14	0.40	0.49	0.80
$\hat{H}_{mov}^{m,0.3}$	FM		0.44	0.13	0.05	0.40	0.82	0.28	0.42	0.53	0.91
	D		0.41	0.11	0.05	0.38	0.80	0.24	0.43	0.54	0.89
	IM		0.21	0.07	0.05	0.31	0.66	0.13	0.41	0.49	0.80
$\hat{H}_{mov,sn}^{m,0.1}$	FM		0.46	0.14	0.06	0.20	0.82	0.32	0.18	0.28	0.89
	D		0.41	0.12	0.06	0.20	0.80	0.29	0.18	0.29	0.88
	IM		0.23	0.07	0.05	0.21	0.69	0.18	0.23	0.34	0.81
$\hat{H}_{mov,sn}^{m,0.2}$	FM		0.45	0.14	0.05	0.20	0.80	0.28	0.17	0.28	0.88
	D		0.40	0.12	0.05	0.20	0.79	0.25	0.18	0.29	0.87
	IM		0.23	0.07	0.05	0.21	0.68	0.16	0.23	0.34	0.79
$\hat{H}_{mov,sn}^{m,0.3}$	FM		0.44	0.14	0.05	0.19	0.80	0.26	0.17	0.28	0.88
	D		0.39	0.12	0.05	0.20	0.78	0.24	0.18	0.29	0.87
	IM		0.23	0.07	0.05	0.21	0.67	0.15	0.23	0.34	0.79

Table 5: Size-corrected power against $I(1)$ breaks for $T = 500$ and $\rho_1 = \rho_2 = 0.6$.

$\rho_1 = \rho_2 = 0.9$			$m = 0.25$			$m = 0.5$			$m = 0.75$		
		r	0.25	0.5	0.75	0.25	0.5	0.75	0.25	0.5	0.75
$\hat{H}^m$	FM		0.09	0.06	0.05	0.23	0.30	0.07	0.27	0.33	0.47
	D		0.09	0.06	0.05	0.24	0.30	0.06	0.29	0.34	0.46
	IM		0.06	0.05	0.05	0.17	0.16	0.05	0.29	0.30	0.33
$\hat{H}_d^m$	FM		0.09	0.06	0.05	0.23	0.30	0.07	0.27	0.32	0.47
	D		0.09	0.06	0.05	0.24	0.30	0.06	0.28	0.33	0.46
	IM		0.06	0.05	0.05	0.17	0.16	0.05	0.29	0.30	0.33
$\hat{H}_{sn}^m$	FM		0.09	0.06	0.05	0.15	0.28	0.07	0.13	0.18	0.42
	D		0.09	0.06	0.05	0.15	0.28	0.07	0.14	0.19	0.41
	IM		0.06	0.05	0.05	0.13	0.17	0.05	0.18	0.23	0.33
$\hat{H}_{mov}^{m,0.1}$	FM		0.09	0.06	0.05	0.22	0.30	0.07	0.28	0.32	0.47
	D		0.09	0.06	0.05	0.23	0.30	0.07	0.29	0.34	0.47
	IM		0.06	0.05	0.05	0.16	0.15	0.05	0.28	0.30	0.33
$\hat{H}_{mov}^{m,0.2}$	FM		0.09	0.06	0.05	0.23	0.30	0.07	0.27	0.33	0.47
	D		0.09	0.06	0.05	0.23	0.30	0.07	0.29	0.34	0.46
	IM		0.06	0.05	0.05	0.16	0.16	0.05	0.29	0.30	0.33
$\hat{H}_{mov}^{m,0.3}$	FM		0.09	0.06	0.05	0.23	0.30	0.07	0.27	0.33	0.47
	D		0.09	0.06	0.05	0.23	0.30	0.06	0.29	0.34	0.46
	IM		0.06	0.05	0.05	0.17	0.16	0.05	0.29	0.30	0.33
$\hat{H}_{mov,sn}^{m,0.1}$	FM		0.09	0.06	0.05	0.14	0.28	0.07	0.13	0.18	0.42
	D		0.09	0.06	0.05	0.15	0.28	0.08	0.14	0.19	0.41
	IM		0.06	0.05	0.05	0.13	0.17	0.06	0.18	0.23	0.33
$\hat{H}_{mov,sn}^{m,0.2}$	FM		0.09	0.06	0.05	0.14	0.28	0.07	0.13	0.18	0.42
	D		0.09	0.06	0.05	0.15	0.28	0.07	0.14	0.19	0.41
	IM		0.06	0.05	0.05	0.13	0.17	0.06	0.18	0.23	0.33
$\hat{H}_{mov,sn}^{m,0.3}$	FM		0.09	0.06	0.05	0.14	0.28	0.07	0.13	0.18	0.42
	D		0.09	0.06	0.05	0.15	0.28	0.07	0.14	0.19	0.41
	IM		0.06	0.05	0.05	0.13	0.17	0.05	0.18	0.23	0.33

Table 6: Size-corrected power against $I(1)$ breaks for $T = 500$ and $\rho_1 = \rho_2 = 0.9$.

Size-Corrected Power – Trend Breaks

The size-corrected power results in case of trend breaks complement the results for the case of I(1) breaks from Section 3 in the main document. The parameter θ_{D_1} varies in 101 equidistant steps over the interval $[1, 1.5]$, including the corresponding null hypothesis value $\theta_{D_1} = 1$. Figure 10 displays size-corrected power against trend breaks using $\hat{H}^m$, $\hat{H}^m_{sn}$, $\hat{H}^{m,0.1}_{mov}$ and $\hat{H}^{m,0.1}_{mov,sn}$. The sample size is $T = 200$, calibration and break fraction are set to $m = 0.5$ and $r = 0.75$ with $\rho_1 = \rho_2 = 0.3$. FM-OLS leads to the highest size-corrected power and IM-OLS to the lowest, with D-OLS in between. Figure 11 displays the corresponding results for $T = 500$. Size-corrected power increases with increasing sample size T. Differences in size-corrected power between FM-OLS and D-OLS become very small for $T = 500$ compared to $T = 200$, reflecting the asymptotic equivalence between FM-OLS and D-OLS. The size-corrected power ranking with respect to FM-OLS, D-OLS and IM-OLS remains unchanged for larger window sizes and other combinations of m and r. Next, consider the impact of different window sizes and in addition the comparison to a detector without moving window. Figure 12 displays size-corrected power for $\hat{H}^m$, $\hat{H}^{m,0.1}_{mov}$, $\hat{H}^{m,0.2}_{mov}$ and $\hat{H}^{m,0.3}_{mov}$ in case of trend breaks. The sample size is $T = 200$ with $\rho_1 = \rho_2 = 0.3$, $m = 0.5$ and $r = 0.75$. Size-corrected power is highest either for $\hat{H}^m$ or $\hat{H}^{m,0.1}_{mov}$. The same holds for other combinations of m and r. Figures 13 and 14 display size-corrected power against trend breaks using $\hat{H}^{m,0.1}_{mov}$ and $\hat{H}^{m,0.1}_{mov,sn}$ and focus on the effect of self-normalization for several combinations of m and r with $\rho_1 = \rho_2 = 0.3$. Self-normalization leads, compared to standardization, by and large to higher size-corrected power for small breaks in θ_{D_1} and to lower size-corrected power for large breaks in θ_{D_1}. For small breaks in θ_{D_1} the differences in size-corrected power between self-normalization and standardization are larger for IM-OLS than for FM-OLS and D-OLS.

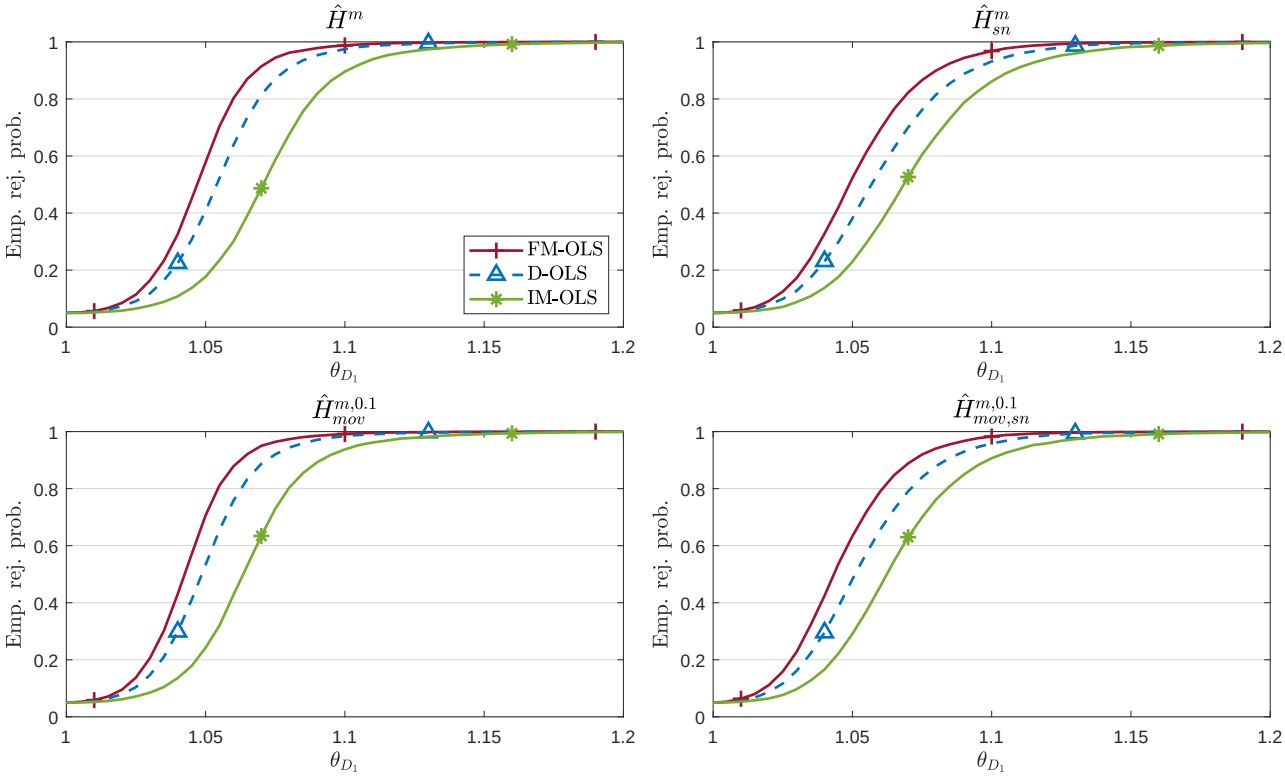

Figure 10: Size-corrected power against trend breaks for $T = 200$, $m = 0.5$, $r = 0.75$ and $\rho_1 = \rho_2 = 0.3$.

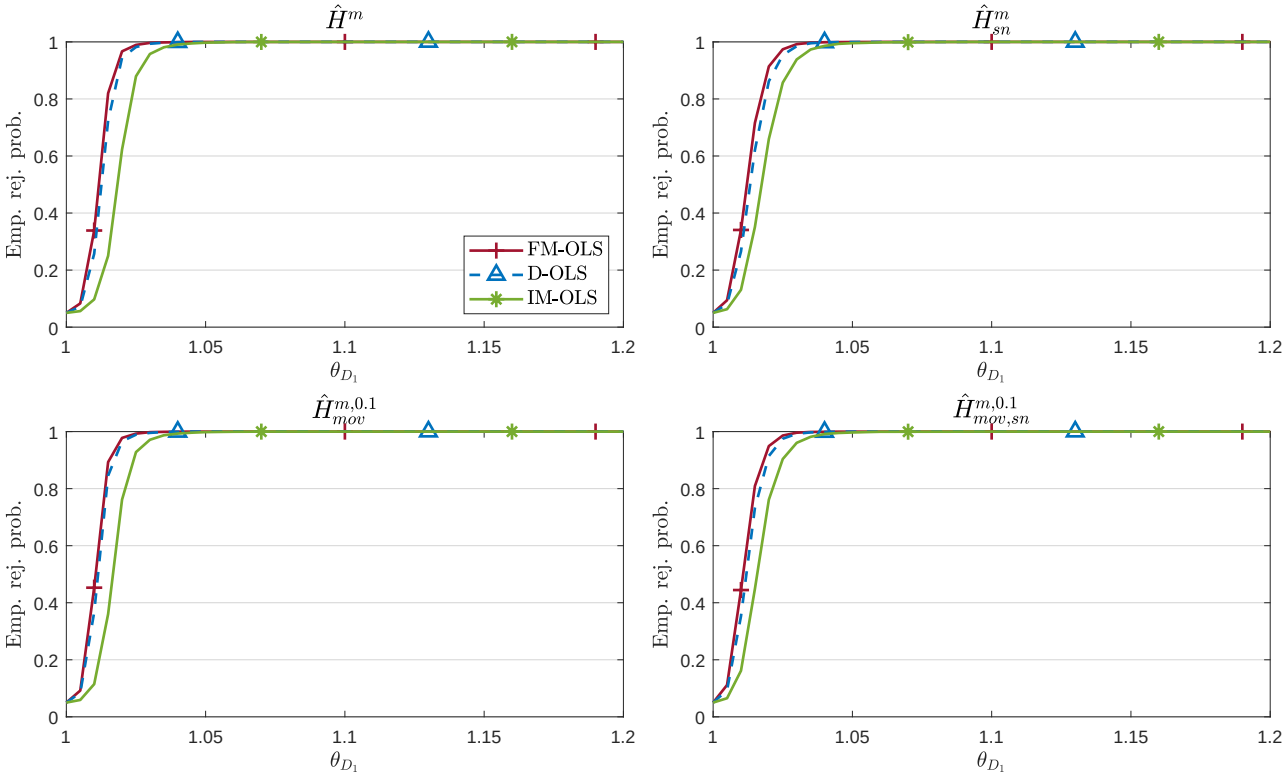

Figure 11: Size-corrected power against trend breaks for $T = 500$, $m = 0.5$, $r = 0.75$ and $\rho_1 = \rho_2 = 0.3$.

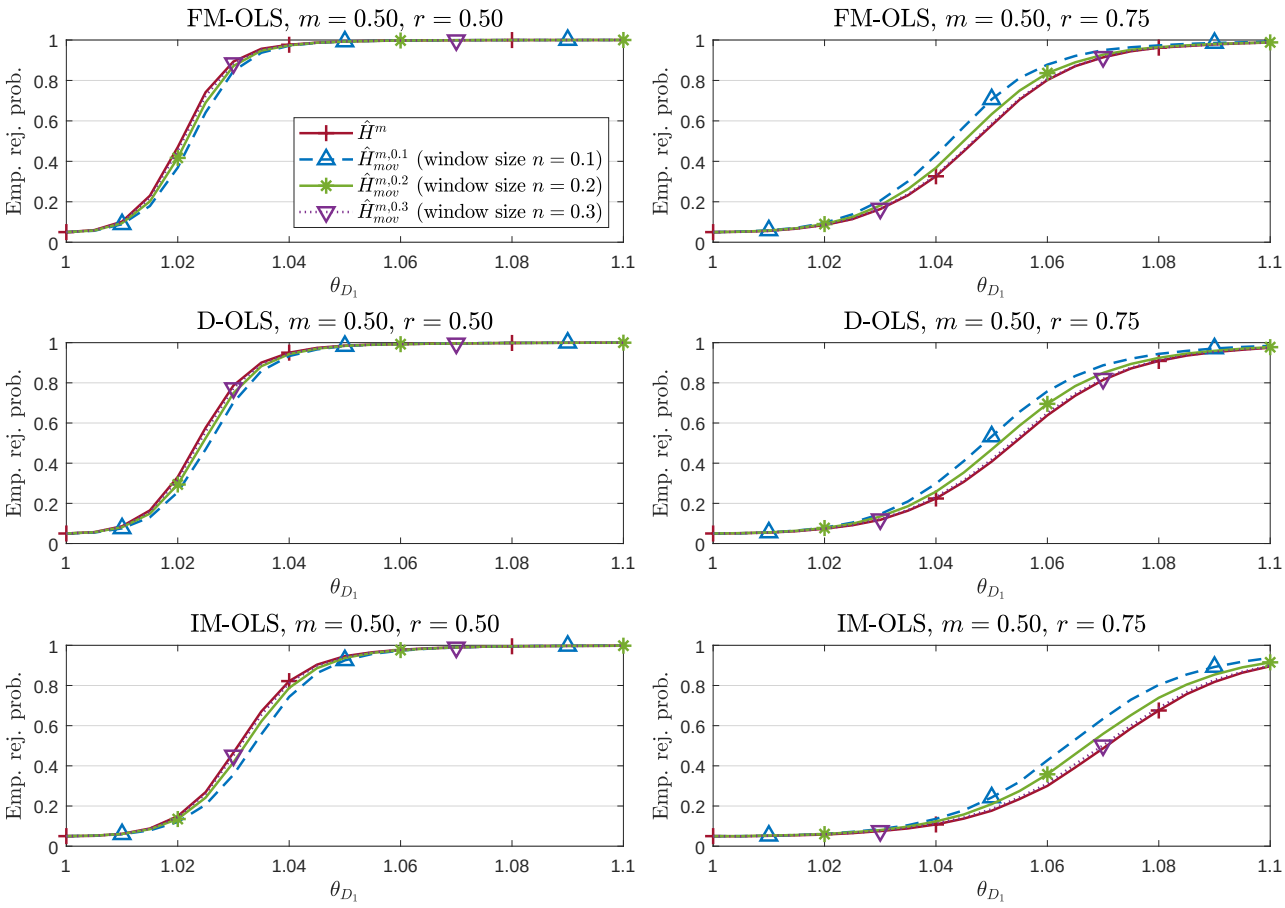

Figure 12: Size-corrected power against trend breaks for $T = 200$ and $\rho_1 = \rho_2 = 0.3$.

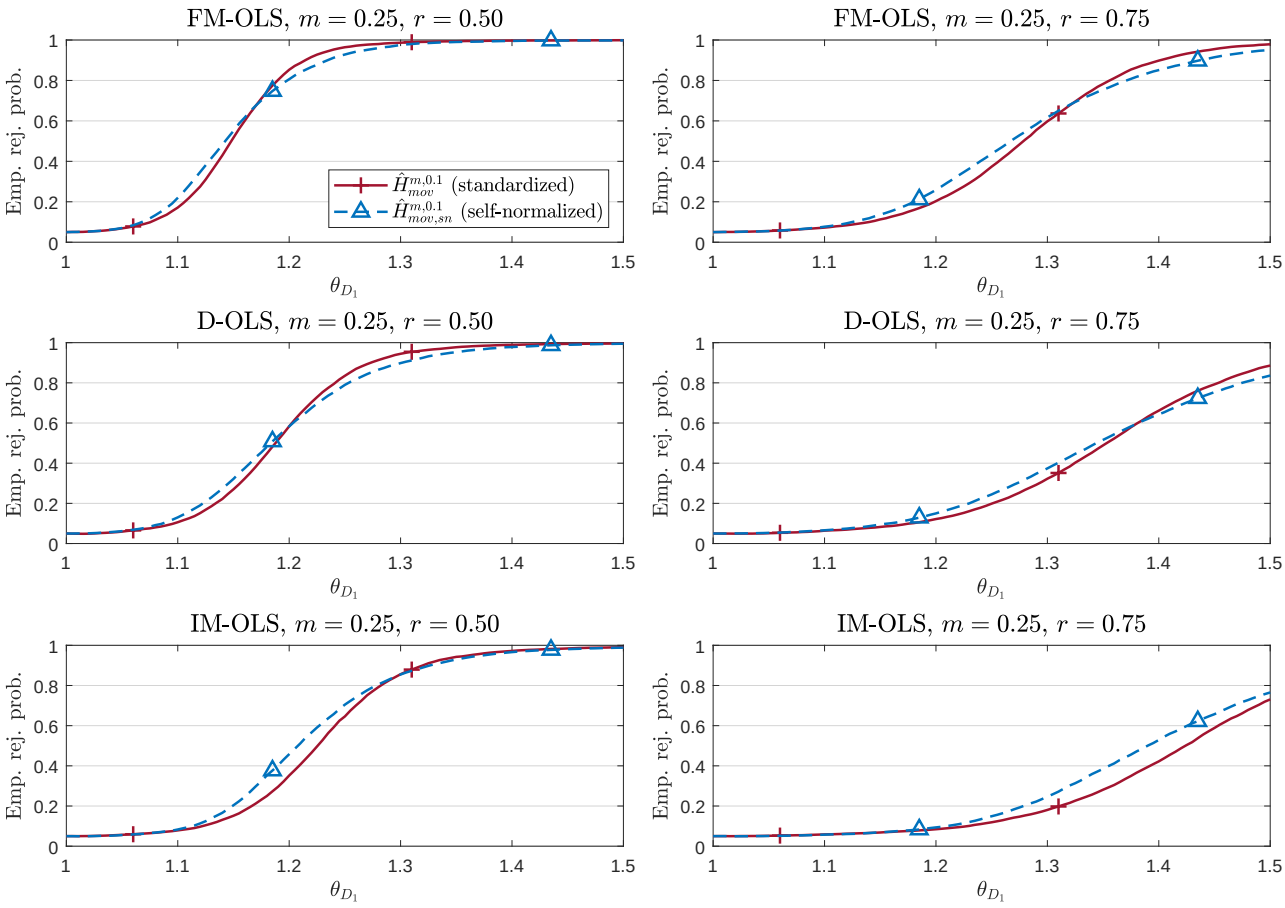

Figure 13: Size-corrected power against trend breaks for $T = 200$ and $\rho_1 = \rho_2 = 0.3$.

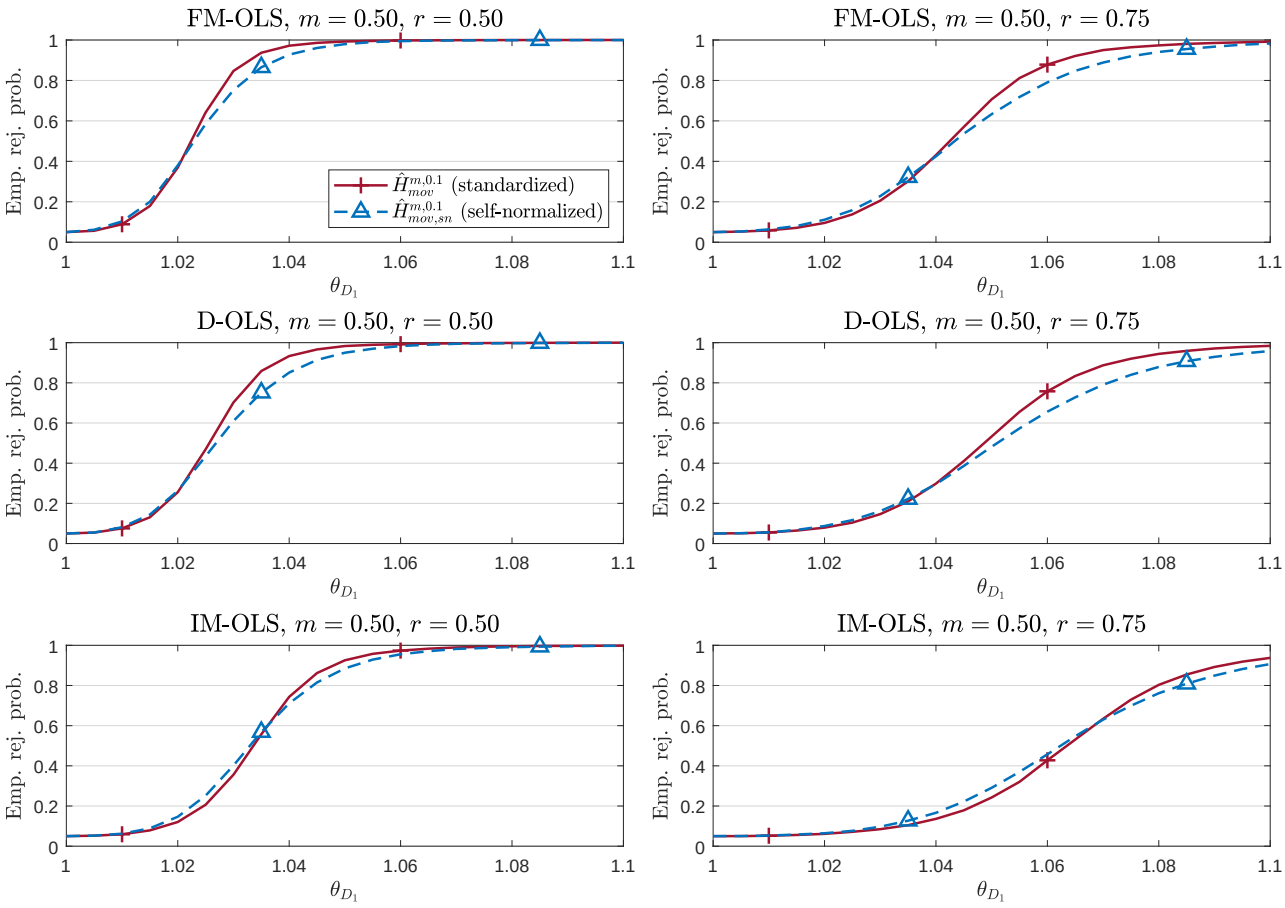

Figure 14: Size-corrected power against trend breaks for $T = 200$ and $\rho_1 = \rho_2 = 0.3$.

Size-Corrected Power – Slope Breaks

We next consider size-corrected power in case of slope breaks, where either $\theta_{X_{1,1}}$ or $\theta_{X_{1,2}}$ changes. The parameter $\theta_{X_{1,1}}$ varies in 26 equidistant steps over the interval $[5, 10]$ and $\theta_{X_{1,2}}$ varies in 27 equidistant steps over the interval $[-0.3, 1]$. The two intervals each include the corresponding null hypothesis value $\theta_{X_{1,1}} = 5$ and $\theta_{X_{1,2}} = -0.3$, respectively. Figures 15 (slope break in $\theta_{X_{1,1}}$) and 16 (slope break in $\theta_{X_{1,2}}$) display size-corrected power for $\hat{H}^m$, $\hat{H}^{m,0.1}_{mov}$, $\hat{H}^{m,0.2}_{mov}$ and $\hat{H}^{m,0.3}_{mov}$. The sample size is $T = 200$ with $\rho_1 = \rho_2 = 0.3$, $m = 0.5$ and $r = 0.75$. Similar to the case of I(1) breaks, size-corrected power is by and large highest for the moving window detector with $n = 0.1$. To assess the impact of self-normalization, Figures 17 ($m = 0.25$) and 18 ($m = 0.5$) display size-corrected power against slope breaks in $\theta_{X_{1,1}}$ using $\hat{H}^{m,0.1}_{mov}$ and $\hat{H}^{m,0.1}_{mov,sn}$, for $T = 200$, $\rho_1 = \rho_2 = 0.3$ and $r \in \{0.5, 0.75\}$. In case of $m = 0.25$, self-normalization leads for small breaks in $\theta_{X_{1,1}}$ to slightly higher size-corrected power than standardization, especially for IM-OLS. In case of $m = 0.5$, standardization leads for FM-OLS and D-OLS to slightly higher size-corrected power than self-normalization, with the exception of very small breaks (i. e. , $\theta_{X_{1,1}} < 5.5$) where both, standardization and self-normalization, lead to equal size-corrected power. For IM-OLS, size-corrected power is almost equal for standardization and self-normalization when $m = 0.5$. The observed results are qualitatively similar for larger sample sizes and other values of ρ_1, ρ_2 and are available upon request.

As expected and already mentioned in the main text, the finite sample size-corrected power results are in line with the results from the LAP analysis in Supplementary Appendix B.

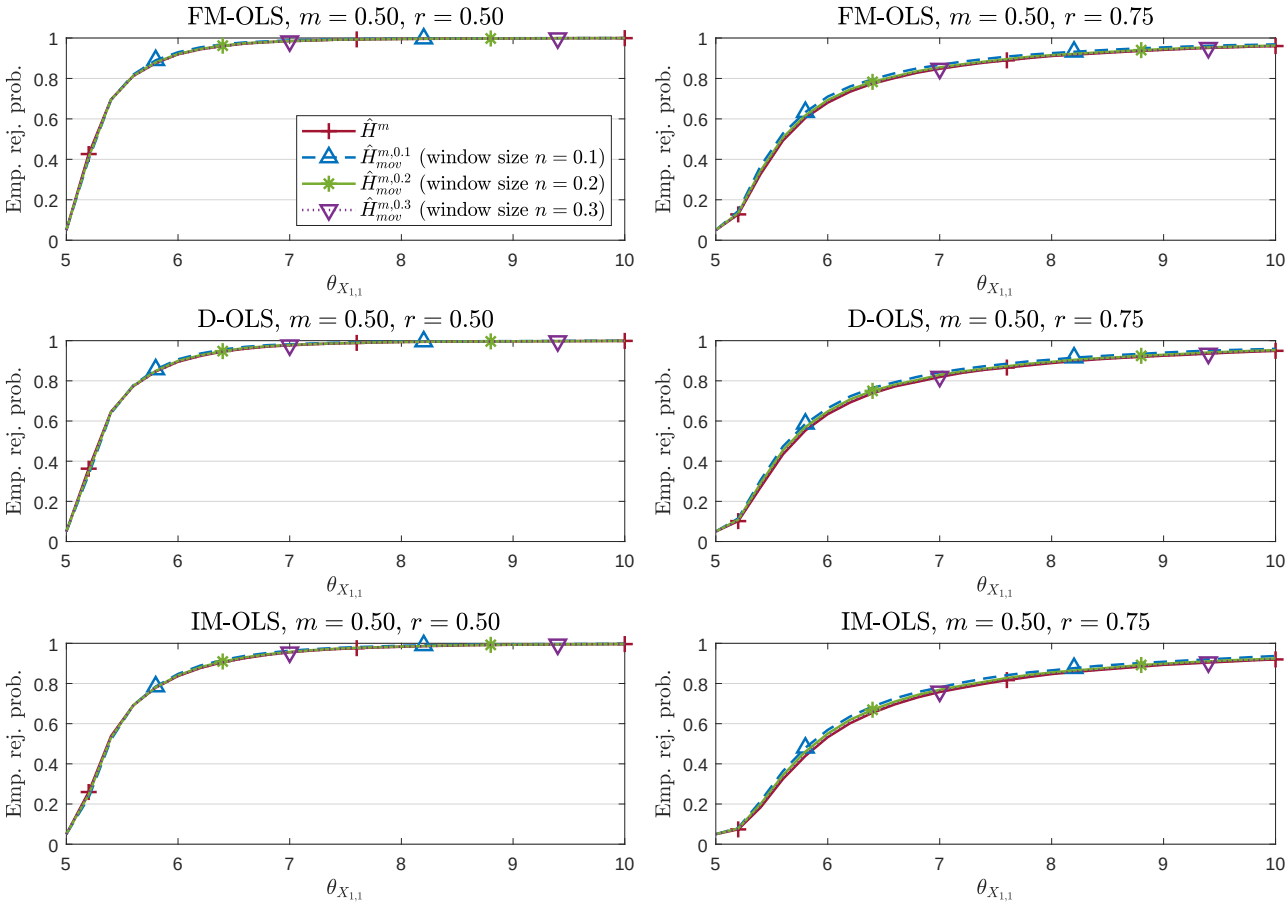

Figure 15: Size-corrected power against slope breaks (in $\theta_{X_{1,1}}$) for $T = 200$ and $\rho_1 = \rho_2 = 0.3$.

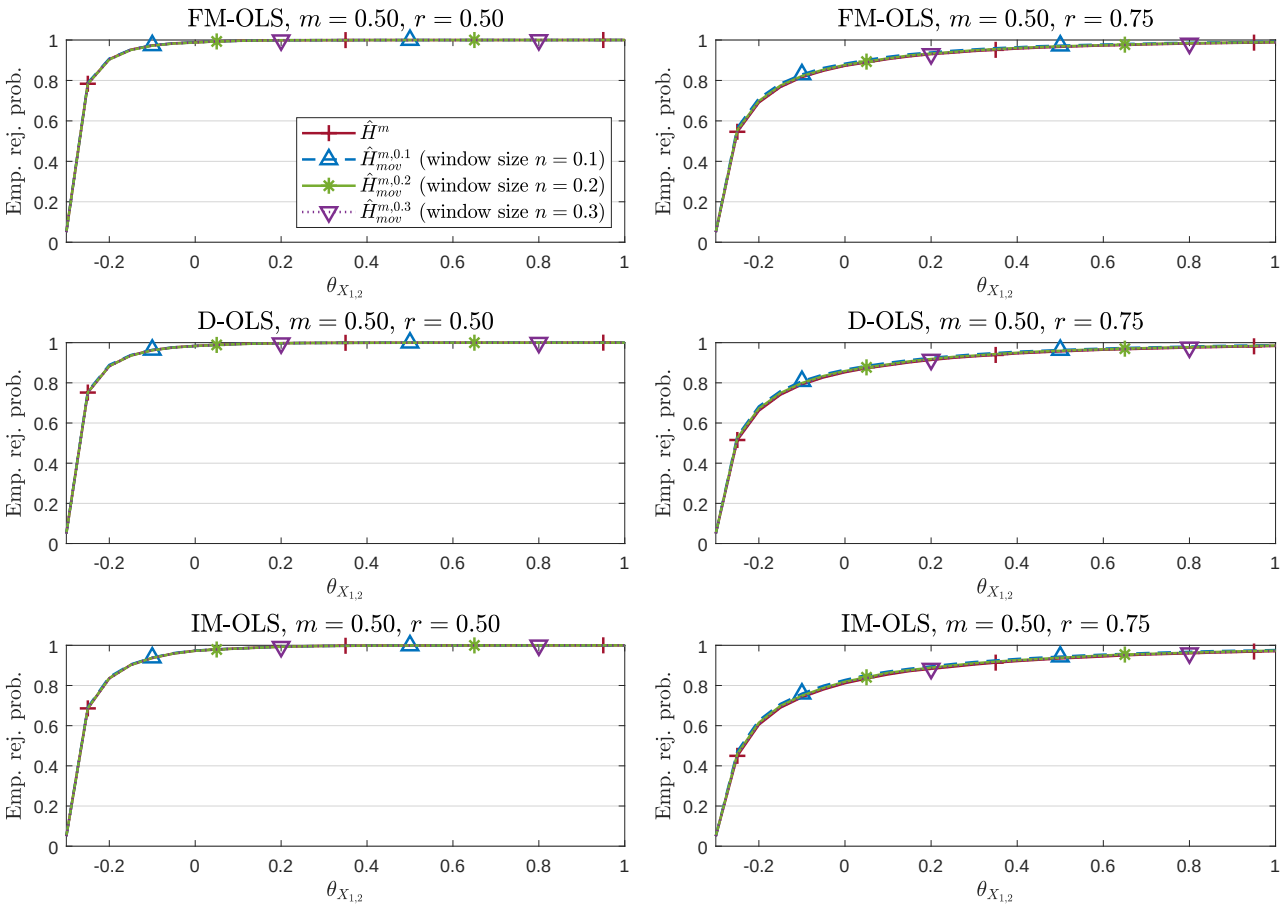

Figure 16: Size-corrected power against slope breaks (in $\theta_{X_{1,2}}$) for $T = 200$ and $\rho_1 = \rho_2 = 0.3$.

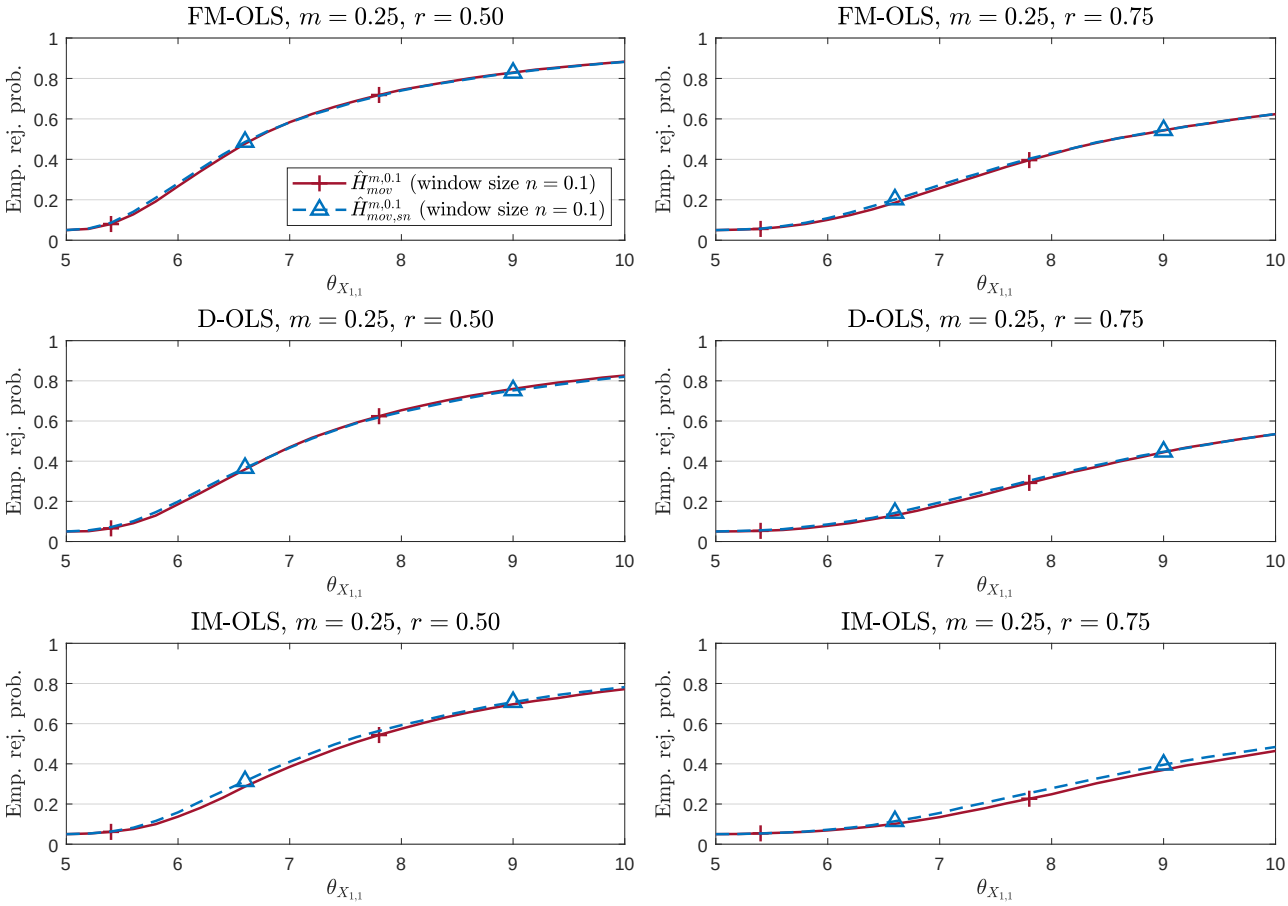

Figure 17: Size-corrected power against slope breaks (in $\theta_{X_{1,1}}$) for $T = 200$ and $\rho_1 = \rho_2 = 0.3$.

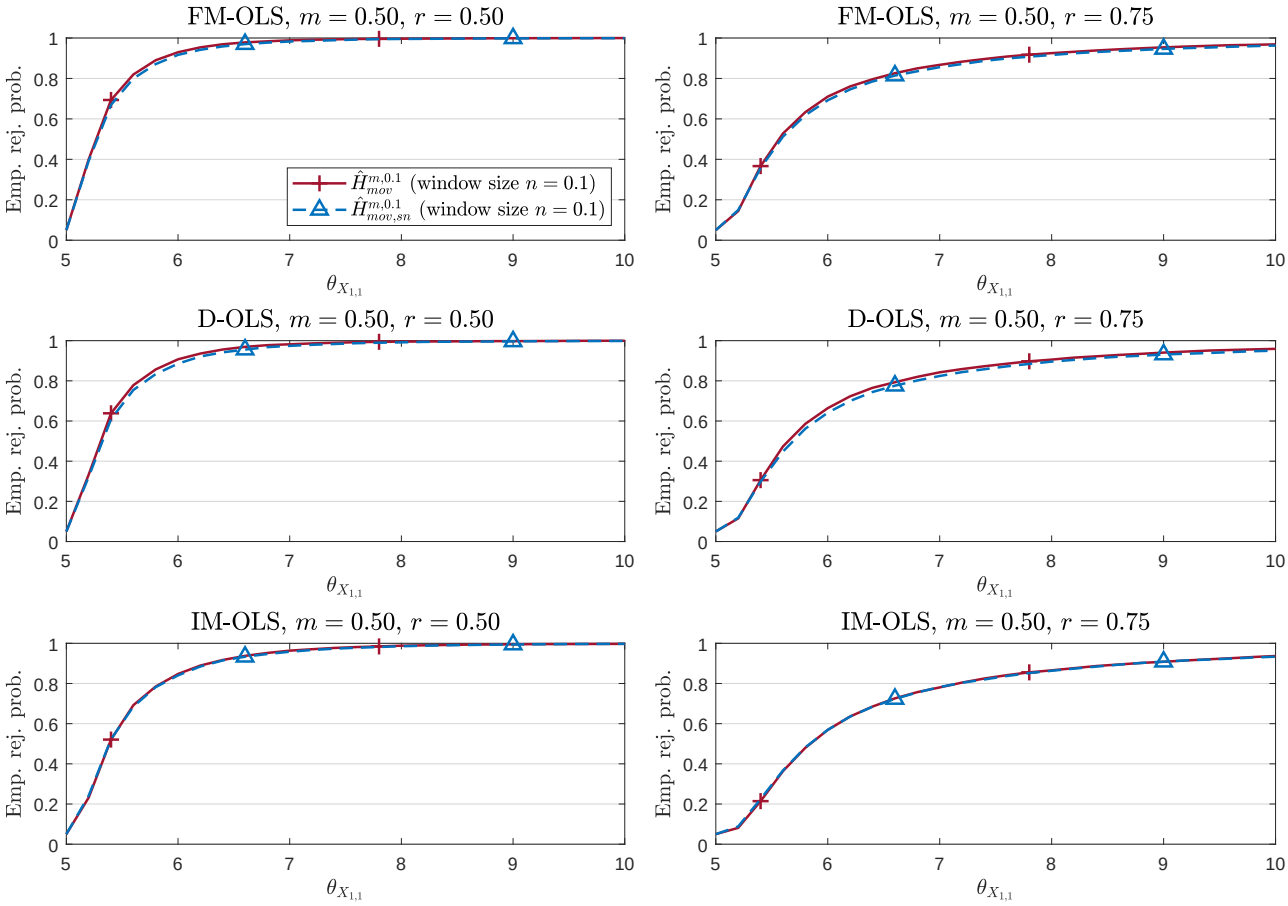

Figure 18: Size-corrected power against slope breaks (in $\theta_{X_{1,1}}$) for $T = 200$ and $\rho_1 = \rho_2 = 0.3$.

Detection Times

We close Supplementary Appendix C with some additional detection time figures. Figure 5 in Section 3 in the main document displays results for $m = 0.5$ and $r = 0.5$ with $T \in \{200, 500\}$ and $\rho_1 = \rho_2 = 0.3$. Figures 19 – 23 here in Supplementary Appendix C complement this figure and display the corresponding results for all other combinations of $m, r \in \{0.25, 0.5, 0.75\}$, with $m \leq r$. In addition, Figure 24 displays detection times for $\rho_1 = \rho_2 = 0.9$, with $m = 0.5$ and $r = 0.5$. As expected, increasing ρ_1, ρ_2 leads to larger delays. Further results, e. g. , for $\rho_1 = \rho_2 = 0$, are available upon request.

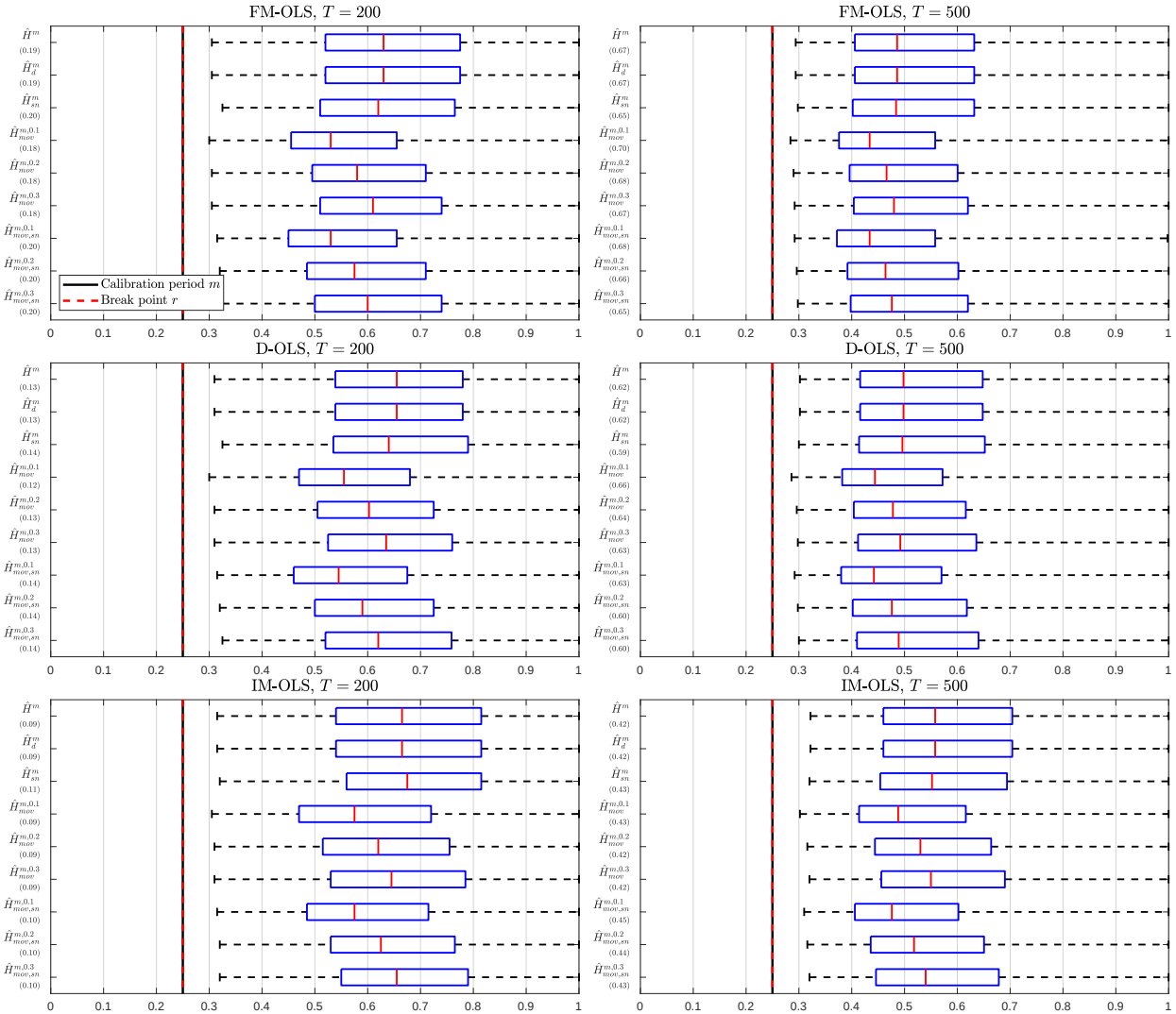

Figure 19: Detection times against $I(1)$ breaks for $m = 0.25$, $r = 0.25$ and $\rho_1 = \rho_2 = 0.3$.

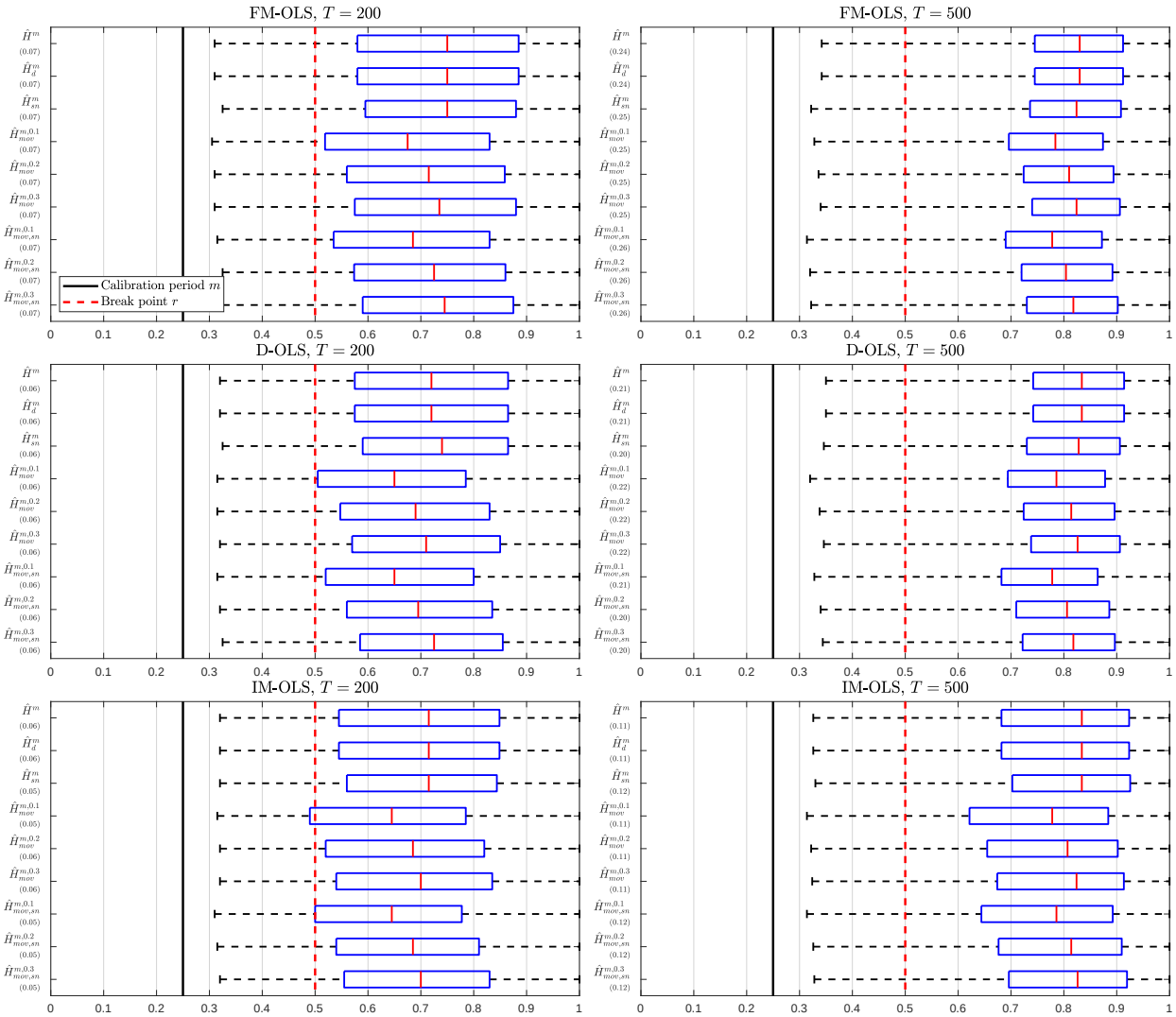

Figure 20: Detection times against $I(1)$ breaks for $m = 0.25$, $r = 0.5$ and $\rho_1 = \rho_2 = 0.3$.

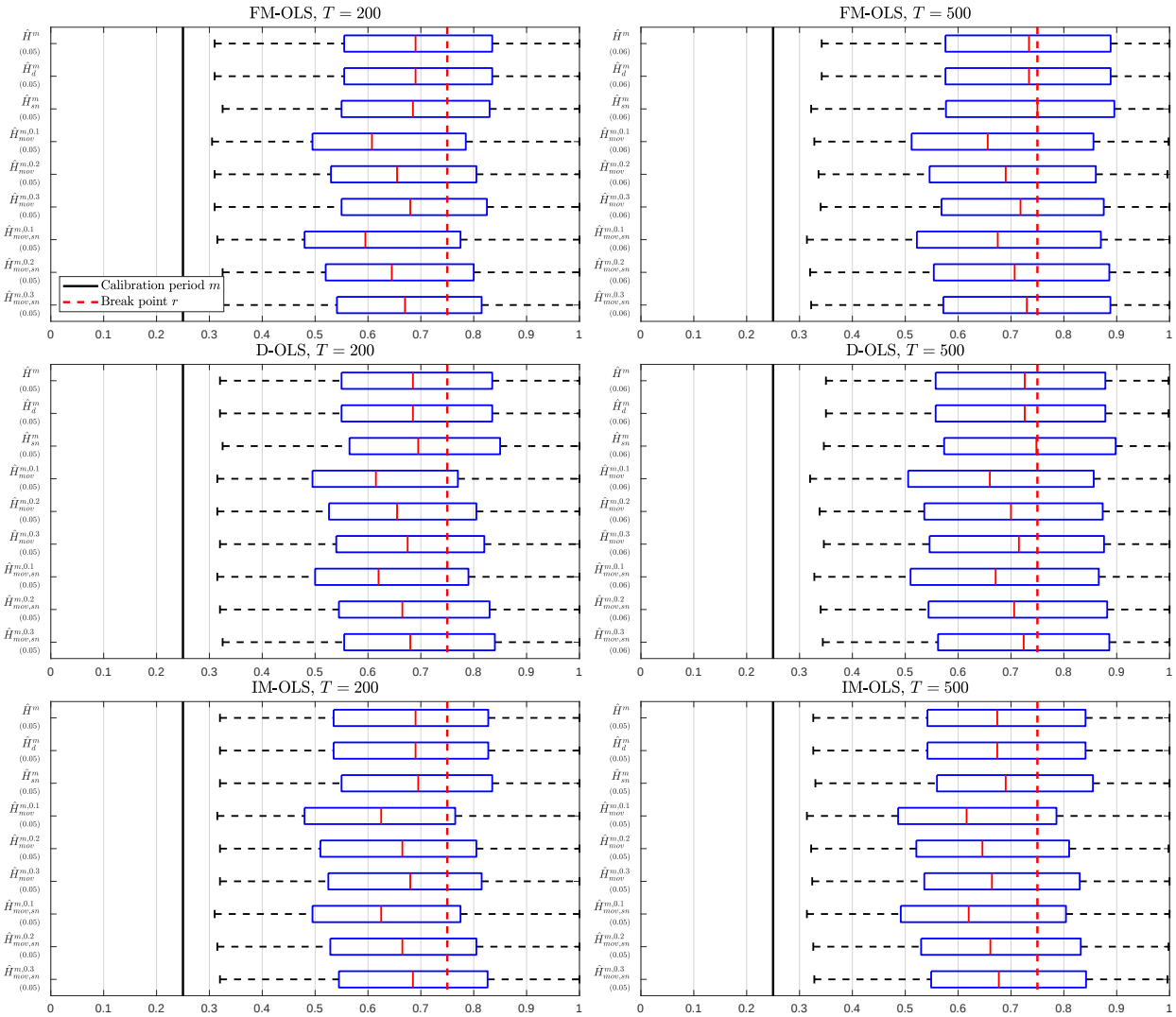

Figure 21: Detection times against $I(1)$ breaks for $m = 0.25$, $r = 0.75$ and $\rho_1 = \rho_2 = 0.3$.

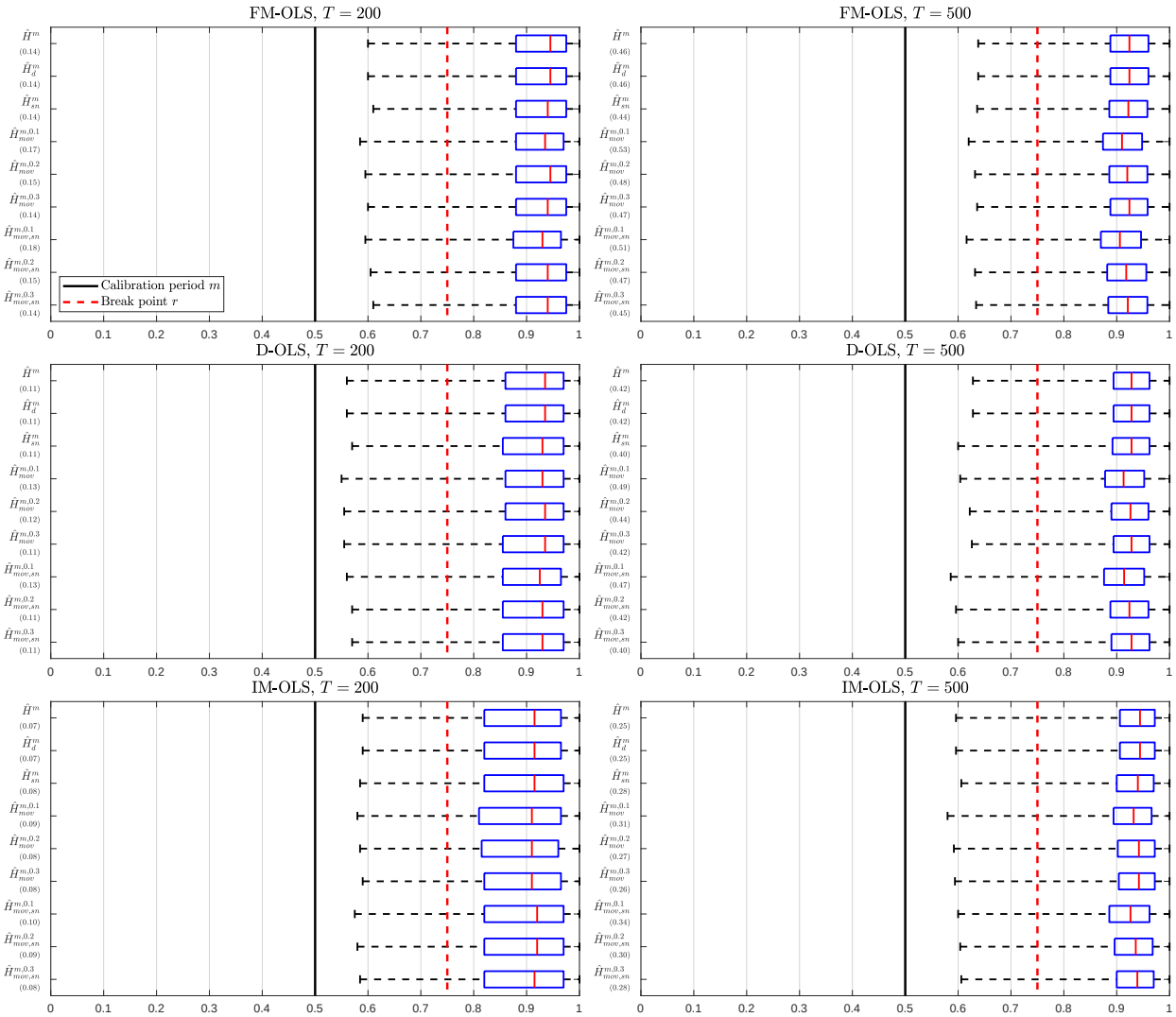

Figure 22: Detection times against $I(1)$ breaks for $m = 0.5$, $r = 0.75$ and $\rho_1 = \rho_2 = 0.3$.

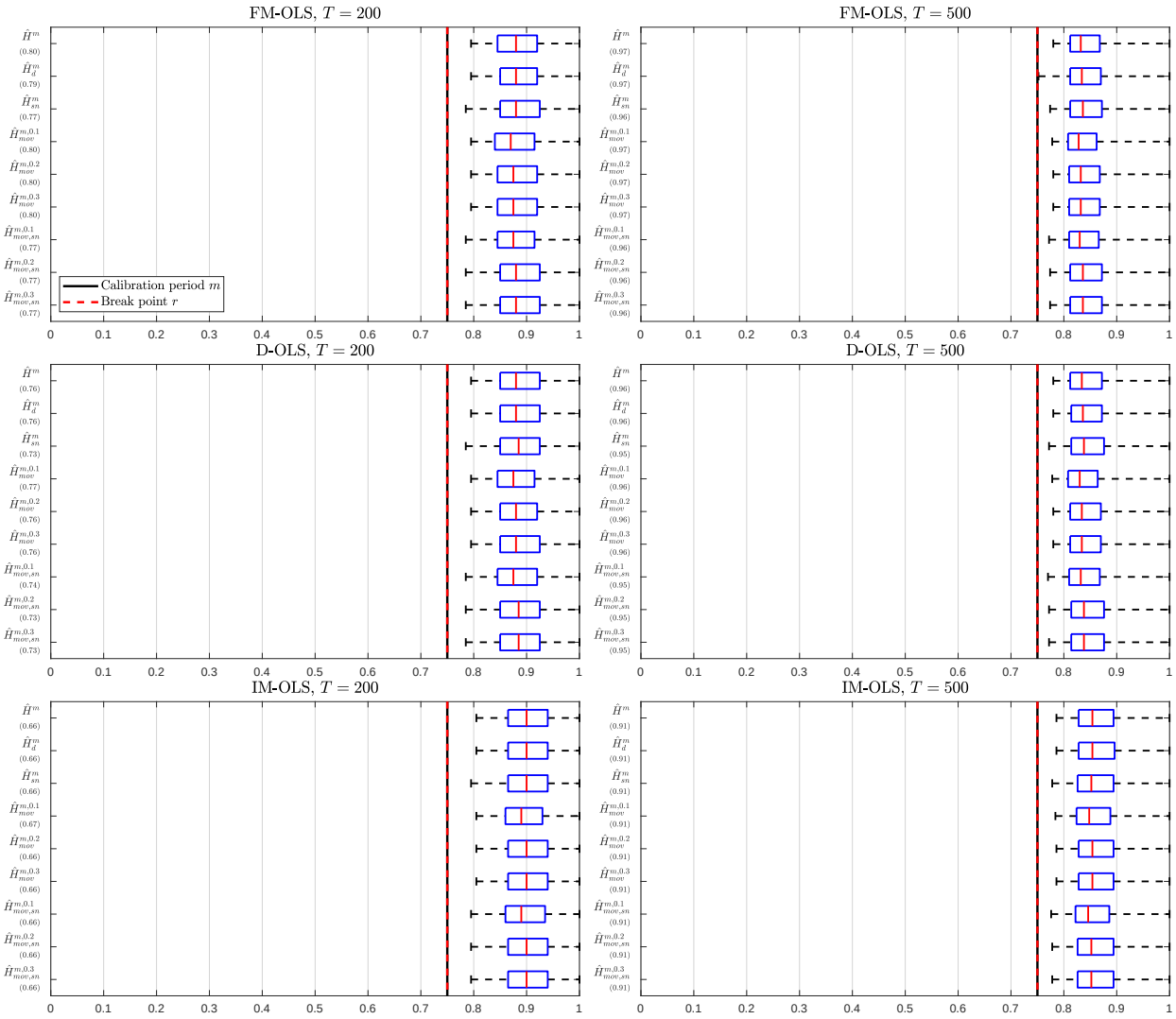

Figure 23: Detection times against $I(1)$ breaks for $m = 0.75$, $r = 0.75$ and $\rho_1 = \rho_2 = 0.3$.

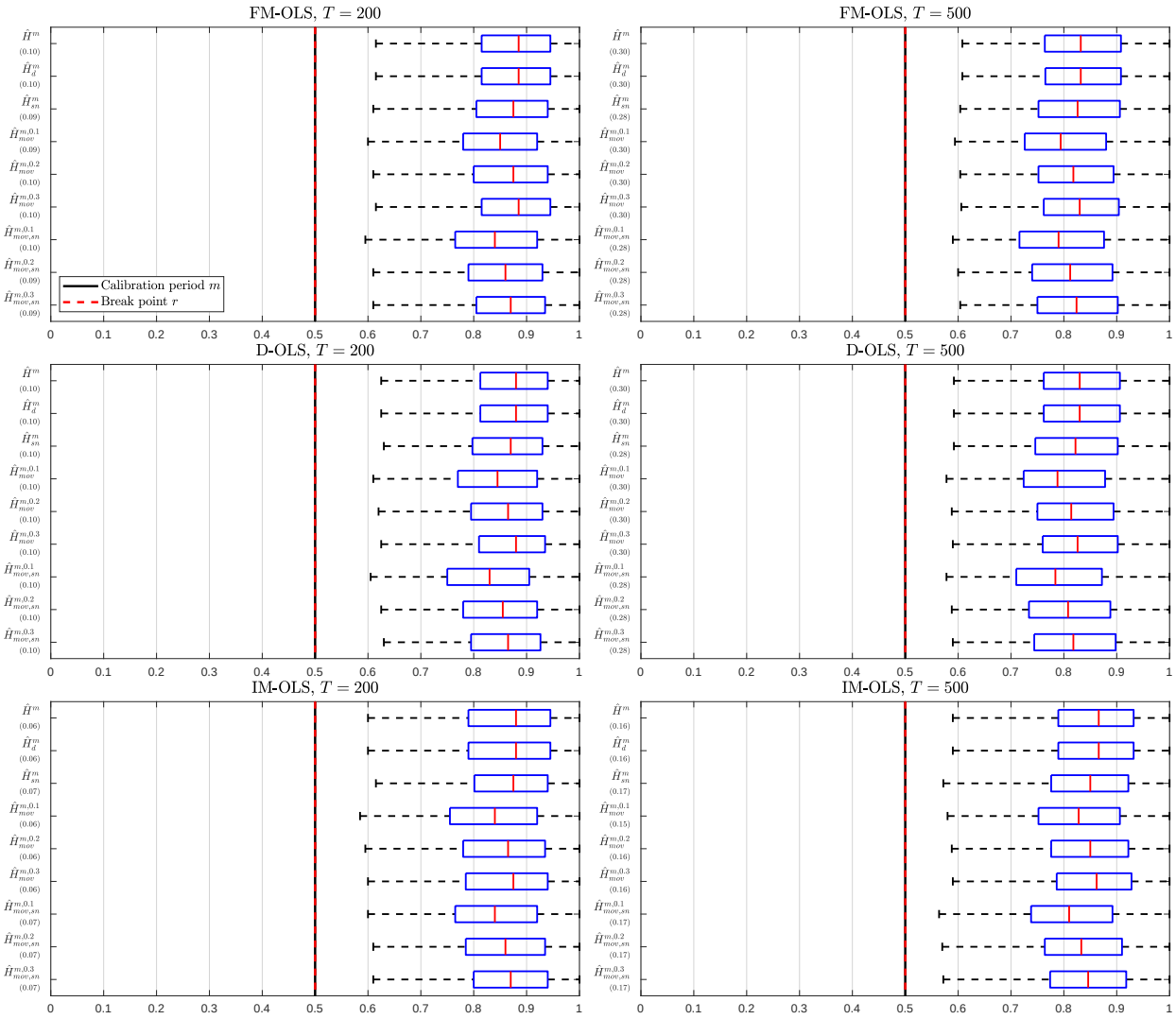

Figure 24: Detection times against $I(1)$ breaks for $m = 0.5$, $r = 0.5$ and $\rho_1 = \rho_2 = 0.9$.

Monitoring Cointegrating Polynomial Regressions

Supplementary Appendix D: Additional Empirical Results

Fabian Knorre, Martin Wagner and Maximilian Grupe

Additional Empirical Results

	ln(GDP)	
Country	ADF	PP
Australia	-1.217	-1.245
Austria	**-7.171**	**-5.324**
Belgium	-0.408	-0.485
Canada	-1.182	-1.044
Denmark	-2.422	-2.629
Finland	-2.178	-2.420
France	**-6.102**	**-3.880**
Germany	**-6.498**	**-5.337**
Italy	*-3.283*	**-4.295**
Japan	-1.724	-1.885
New Zealand	**-5.436**	**-6.237**
Norway	**-5.173**	**-5.221**
Portugal	-0.558	2.010
Spain	-2.415	-2.603
Sweden	-2.460	-2.775
Switzerland	**-5.356**	**-6.322**
United Kingdom	-3.221	*-3.384*
United States	-2.301	-2.547

Table 7: Results of the augmented Dickey and Fuller (1981) and Phillips and Perron (1988) unit root tests for log per capita GDP for the calibration period 1946–1973. The test equation includes intercept and linear trend. For the ADF test, we choose the lag length using the AIC criterion and the maximum lag length is three. *Italic* entries indicate rejection of the null hypothesis at the 10% level and **bold** entries rejection at the 5% level.

	ln(GDP)	
Country	ADF	PP
Australia	-1.146	-1.392
Austria	-2.457	**-5.292**
Belgium	0.123	0.046
Canada	-0.351	-0.377
Denmark	-0.429	-0.440
Finland	-1.151	-0.199
France	-2.069	-2.061
Germany	**-6.960**	**-32.623**
Italy	-0.670	-2.278
Japan	-1.143	-0.878
New Zealand	-2.757	**-3.581**
Norway	1.198	0.733
Portugal	0.089	0.391
Spain	0.505	0.974
Sweden	-1.900	-1.999
Switzerland	-2.154	-1.101
United Kingdom	-1.999	-1.197
United States	-1.303	-1.484

Table 8: Results of the augmented Dickey and Fuller (1981) and Phillips and Perron (1988) unit root tests for log per capita GDP for the full sample period 1946–2016. For further explanations see notes to Table 7.

	$p = 1$			$p = 2$	$p = 3$
	Shin	Johansen		CT	CT
Country		r = 0	r = 1		
Australia	0.075	**73.986**	5.418	0.079	0.055
Belgium	0.035	*23.343*	2.296	0.024	0.028
Canada	0.072	23.197	7.070	*0.091*	0.048
Denmark	0.056	21.761	3.702	0.057	0.056
Finland	**0.147**	12.999	3.362	0.058	0.040
Italy	0.076	*23.399*	5.211	0.065	0.025
Japan	0.045	**37.190**	3.672	0.021	0.025
Portugal	0.052	**43.125**	7.614	0.049	0.036
Spain	*0.099*	*25.045*	10.510	0.061	0.049
Sweden	0.044	*24.473*	6.706	0.034	0.033
United Kingdom	0.072	**30.967**	9.082	0.079	0.053
United States	**0.149**	**26.274**	5.105	0.057	0.049

Table 9: Results of the Shin (1994), Johansen (1995) and CT (Wagner, 2020) tests for log per capita CO_2 emissions and log per capita GDP. The (calibration) period is 1946–1973. For the Johansen test the number of lags is determined using the AIC and the maximum lag length is three. *Italic* entries indicate rejection of the null hypothesis at the 10% level and **bold** entries rejection at the 5% level.

	$p = 1$			$p = 2$	$p = 3$
	Shin	Johansen		CT	CT
Country		r = 0	r = 1		
Australia	0.060	**38.564**	*11.952*	0.059	0.055
Belgium	*0.100*	11.945	2.082	*0.104*	0.022
Canada	0.047	**29.940**	5.195	0.046	0.022
Denmark	**0.137**	17.271	4.976	0.086	0.033
Finland	**0.132**	*23.552*	5.571	0.063	0.031
Italy	*0.111*	**35.603**	5.176	*0.091*	0.028
Japan	**0.145**	14.479	5.003	0.059	0.049
Portugal	0.085	**29.134**	3.959	0.064	0.068
Spain	*0.099*	*25.004*	4.024	0.082	0.076
Sweden	**0.178**	**25.901**	8.170	0.053	0.050
United Kingdom	0.095	**26.260**	4.719	0.054	0.046
United States	**0.142**	**38.707**	**13.683**	**0.113**	0.047

Table 10: Results of the Shin (1994), Johansen (1995) and CT (Wagner, 2020) tests for log per capita SO_2 emissions and log per capita GDP. The (calibration) period is 1946–1973. For further explanations see notes to Table 9.

	Polynomial degree	
Country	CO_2	SO_2
Australia	2	1
Belgium	1	1
Canada	1	1
Denmark	1	3
Finland	1	1
Italy	2	1
Japan	1	2
Portugal	2	1
Spain	1	1
Sweden	1	1
United Kingdom	2	3
United States	1	1

Table 11: Minimal polynomial degrees for cointegrating EKCs over the full sample period 1946–2016. The detailed cointegration test results are available in Tables 12 and 13.

	$p_1 = 1$			$p_1 = 2$	$p_1 = 3$
	Shin	Johansen		CT	CT
Country		r = 0	r = 1		
Australia	**0.165**	**55.183**	9.001	0.047	0.048
Belgium	0.087	22.624	7.421	0.073	0.058
Canada	0.057	22.511	3.539	0.055	0.053
Denmark	0.039	**30.477**	10.229	0.030	0.033
Finland	0.068	**31.796**	**14.518**	0.051	0.056
Italy	**0.121**	**27.923**	4.408	0.082	*0.089*
Japan	*0.111*	**28.798**	7.611	0.073	0.049
Portugal	**0.129**	9.548	3.273	0.057	0.067
Spain	0.055	23.116	6.730	0.056	0.052
Sweden	0.050	**29.520**	*10.818*	0.076	0.054
United Kingdom	**0.200**	**35.167**	7.089	0.068	0.041
United States	*0.102*	20.504	5.966	0.067	0.065

Table 12: Results of the Shin (1994), Johansen (1995) and CT (Wagner, 2020) tests for log per capita CO_2 emissions and log per capita GDP. The (full sample) period is 1946–2016. For further explanations see notes to Table 9.

	$p_1 = 1$			$p_1 = 2$	$p_1 = 3$
	Shin	Johansen		CT	CT
Country		r = 0	r = 1		
Australia	0.064	20.417	3.540	0.047	0.036
Belgium	*0.116*	20.564	4.520	0.062	0.033
Canada	*0.105*	**29.641**	*12.067*	0.060	0.071
Denmark	0.084	**28.038**	4.788	**0.107**	0.057
Finland	*0.109*	14.953	5.029	*0.096*	*0.100*
Italy	*0.101*	**40.453**	3.823	0.070	0.050
Japan	**0.127**	**40.635**	9.440	0.064	0.066
Portugal	*0.100*	13.291	5.239	0.068	0.077
Spain	0.089	18.603	8.650	*0.088*	0.070
Sweden	0.067	*23.999*	8.783	*0.097*	0.071
United Kingdom	**0.213**	**33.910**	9.928	**0.122**	0.065
United States	0.080	**32.551**	**14.114**	0.041	0.041

Table 13: Results of the Shin (1994), Johansen (1995) and CT (Wagner, 2020) tests for log per capita SO_2 emissions and log per capita GDP. The (full sample) period is 1946–2016. For further explanations see notes to Table 9.

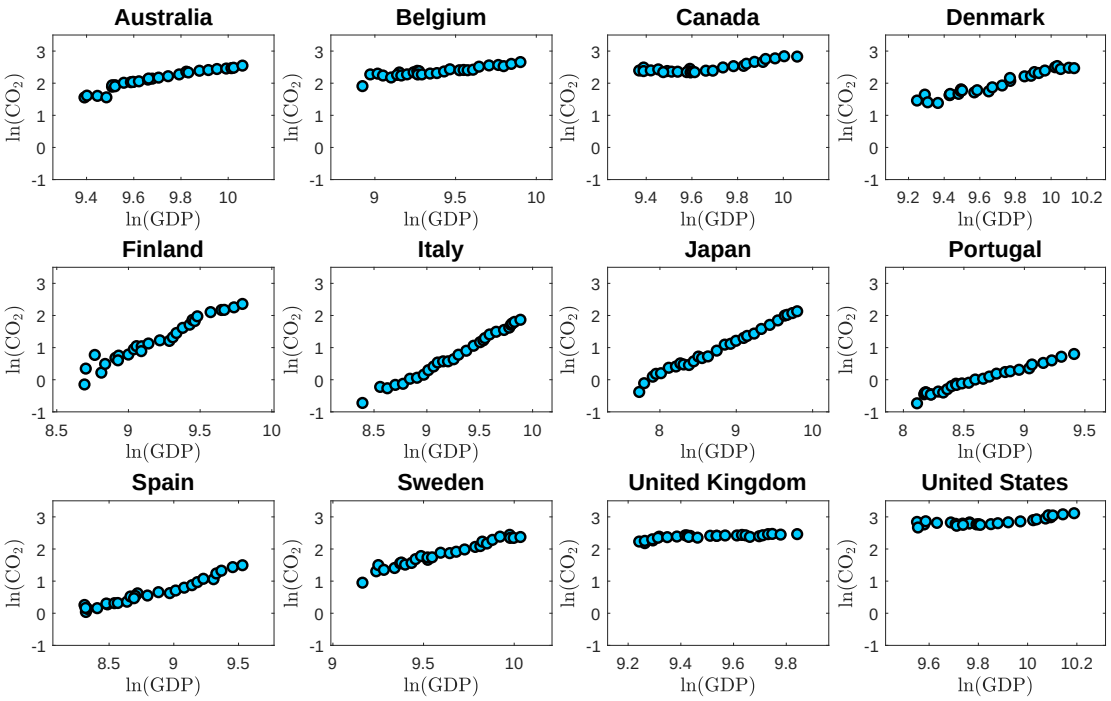

Figure 25: The scatter plots show pairs of observations of log per capita GDP and log per capita CO_2 emissions for the calibration period 1946–1973 for the considered twelve countries.

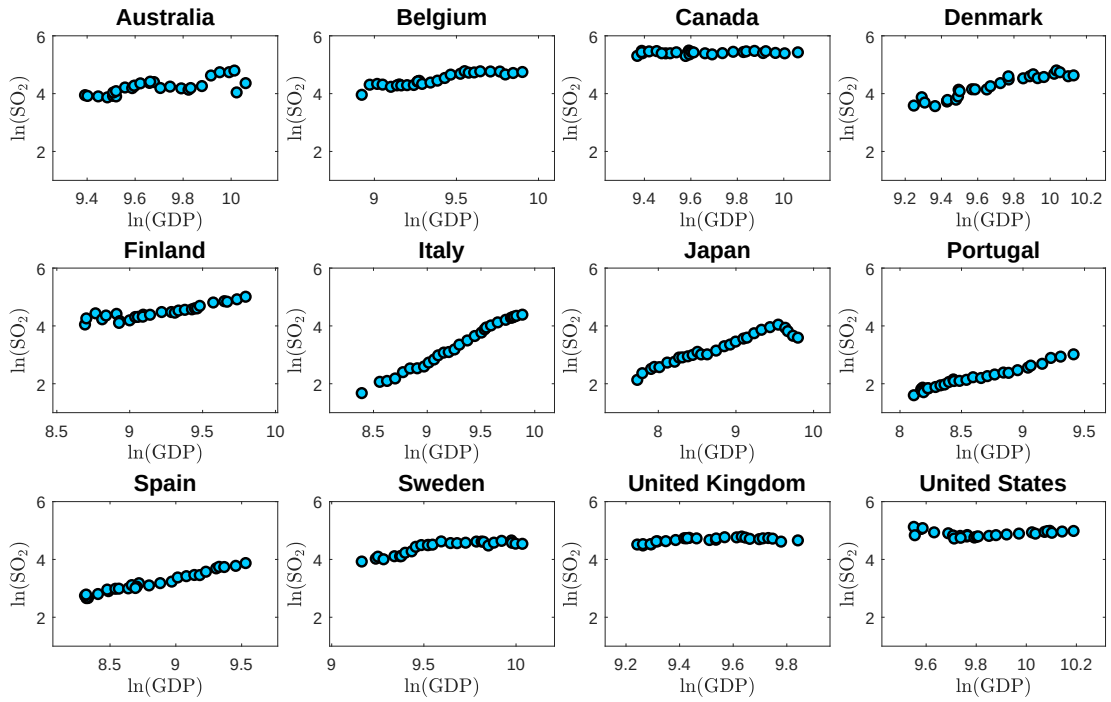

Figure 26: The scatter plots show pairs of observations of log per capita GDP and log per capita SO_2 emissions for the calibration period 1946–1973 for the considered twelve countries.

		$\hat{H}^{m}$			$\hat{H}^{m}_{d}$			$\hat{H}^{m}_{sn}$			$\hat{H}^{m,0.1}_{mov}$			$\hat{H}^{m,0.2}_{mov}$			$\hat{H}^{m,0.3}_{mov}$			$\hat{H}^{m,0.1}_{mov,sn}$			$\hat{H}^{m,0.2}_{mov,sn}$			$\hat{H}^{m,0.3}_{mov,sn}$		
Country	p	FM	D	IM	FM	D	IM	FM	D	IM	FM	D	IM	FM	D	IM	FM	D	IM	FM	D	IM	FM	D	IM	FM	D	IM
Australia	1	1993	1993	2001	1993	1993	2001	1997	2001	2006	1990	1990	1997	1992	1992	1999	1993	1992	2001	1993	1997	2001	1995	1999	2003	1996	2000	2005
Belgium	1	1993	1992	2001	1993	1992	2001	1991	1990	1998	1989	1989	1993	1992	1991	1997	1993	1992	1999	1988	1988	1992	1990	1989	1995	1991	1990	1997
Canada	1	∞	∞	∞	∞	∞	∞	∞	1986	∞	∞	∞	∞	∞	∞	∞	∞	∞	∞	∞	1982	∞	∞	1985	∞	∞	1986	∞
Denmark	1	1993	1991	2006	1993	1991	2006	1996	1992	2014	1989	1988	2003	1992	1990	2004	1993	1991	2005	1991	1988	2011	1994	1990	2012	1995	1991	2013
Finland	2	1990	1997	1992	1990	1997	1992	1992	2000	1993	1988	1994	1989	1989	1996	1991	1990	1997	1991	1989	1996	1990	1991	1998	1992	1992	1999	1993
Italy	1	1982	1982	1983	1982	1982	1983	1983	1982	1984	1980	1981	1981	1981	1982	1982	1981	1982	1983	1981	1980	1982	1983	1981	1983	1983	1981	1983
Japan	1	1985	1984	1985	1985	1984	1985	1985	1982	1982	1982	1981	1982	1984	1983	1984	1985	1983	1984	1982	1980	1980	1984	1981	1981	1985	1981	1982
Portugal	1	2000	∞	∞	2000	∞	∞	2002	∞	∞	1996	∞	∞	1998	∞	∞	1999	∞	∞	1998	∞	∞	2000	∞	∞	2001	∞	∞
Spain	1	∞	∞	∞	∞	∞	∞	∞	∞	∞	∞	∞	∞	∞	∞	∞	∞	∞	∞	∞	∞	∞	∞	∞	∞	∞	∞	∞
Sweden	1	1983	1982	1985	1984	1982	1985	1983	1983	1985	1982	1981	1983	1983	1982	1984	1983	1982	1985	1982	1981	1983	1983	1982	1985	1983	1982	1985
United Kingdom	1	1984	1988	1988	1984	1988	1988	1986	1985	1991	1982	1986	1985	1983	1987	1987	1984	1988	1988	1984	1983	1987	1985	1985	1989	1986	1985	1991
United States	2	1989	1989	1992	1989	1989	1992	1990	1990	1995	1987	1987	1990	1988	1988	1992	1988	1989	1992	1988	1988	1992	1989	1990	1994	1990	1990	1994

Table 14: Detection times when monitoring CO_2 emissions using all nine detectors and all three estimation methods FM-OLS, D-OLS and IM-OLS. The column p indicates the polynomial degree, the calibration period is 1946–1973, the monitoring period is 1974–2016. The nominal significance level is 5%.

		$\hat{H}^{m}$			$\hat{H}^{m}_{d}$			$\hat{H}^{m}_{sn}$			$\hat{H}^{m,0.1}_{mov}$			$\hat{H}^{m,0.2}_{mov}$			$\hat{H}^{m,0.3}_{mov}$			$\hat{H}^{m,0.1}_{mov,sn}$			$\hat{H}^{m,0.2}_{mov,sn}$			$\hat{H}^{m,0.3}_{mov,sn}$		
Country	p	FM	D	IM	FM	D	IM	FM	D	IM	FM	D	IM	FM	D	IM	FM	D	IM	FM	D	IM	FM	D	IM	FM	D	IM
Australia	1	∞	∞	∞	∞	∞	∞	∞	∞	∞	∞	∞	∞	∞	∞	∞	∞	∞	∞	∞	∞	∞	∞	∞	∞	∞	∞	∞
Belgium	1	1984	1984	1985	1984	1984	1985	1987	1986	1988	1983	1982	1983	1984	1983	1984	1984	1984	1985	1985	1984	1985	1986	1985	1987	1987	1986	1987
Canada	1	1981	1981	1982	1981	1981	1982	1981	1982	1982	1980	1980	1980	1981	1981	1981	1981	1981	1982	1980	1981	1981	1981	1982	1982	1981	1982	1982
Denmark	2	1994	1999	2007	1994	1999	2007	1999	1990	2009	1991	1997	2005	1993	1998	2006	1993	1999	2006	1997	1987	2006	1998	1989	2008	1999	1990	2008
Finland	2	1988	1987	1991	1988	1987	1991	1990	1987	1993	1986	1985	1989	1988	1987	1990	1988	1987	1990	1988	1986	1991	1989	1987	1992	1990	1987	1993
Italy	1	1981	1981	1982	1981	1981	1982	1984	1984	1984	1980	1979	1980	1981	1980	1981	1981	1981	1982	1982	1982	1982	1983	1983	1983	1984	1983	1984
Japan	2	1991	2005	2004	1991	2005	2004	1993	2007	2007	1989	2002	2002	1991	2004	2003	1991	2004	2004	1991	2005	2004	1992	2007	2006	1993	2007	2007
Portugal	1	2015	2013	∞	2015	2013	∞	∞	∞	∞	2013	2012	2015	2014	2013	∞	2015	2013	∞	2015	2015	∞	∞	2016	∞	∞	∞	∞
Spain	1	2003	2002	2011	2003	2002	2011	2007	2007	2013	1983	1983	1984	1986	2002	1987	2003	2002	2011	2005	2005	2012	2007	2007	2013	2007	2007	2014
Sweden	2	1986	1986	1989	1986	1986	1989	1987	1988	1990	1984	1984	1987	1985	1986	1988	1986	1986	1989	1985	1986	1988	1986	1988	1989	1986	1988	1990
United Kingdom	1	1982	1983	1984	1982	1983	1984	1985	1989	1985	1981	1981	1982	1982	1982	1983	1982	1983	1983	1983	1985	1983	1984	1987	1984	1985	1988	1985
United States	3	∞	∞	∞	∞	∞	∞	∞	∞	∞	∞	∞	∞	∞	∞	∞	∞	∞	∞	∞	∞	∞	∞	∞	∞	∞	∞	∞

Table 15: Detection times when monitoring SO_2 emissions using all nine detectors and all three estimation methods FM-OLS, D-OLS and IM-OLS. The column p indicates the polynomial degree, the calibration period is 1946–1973, the monitoring period is 1974–2016. The nominal significance level is 5%.

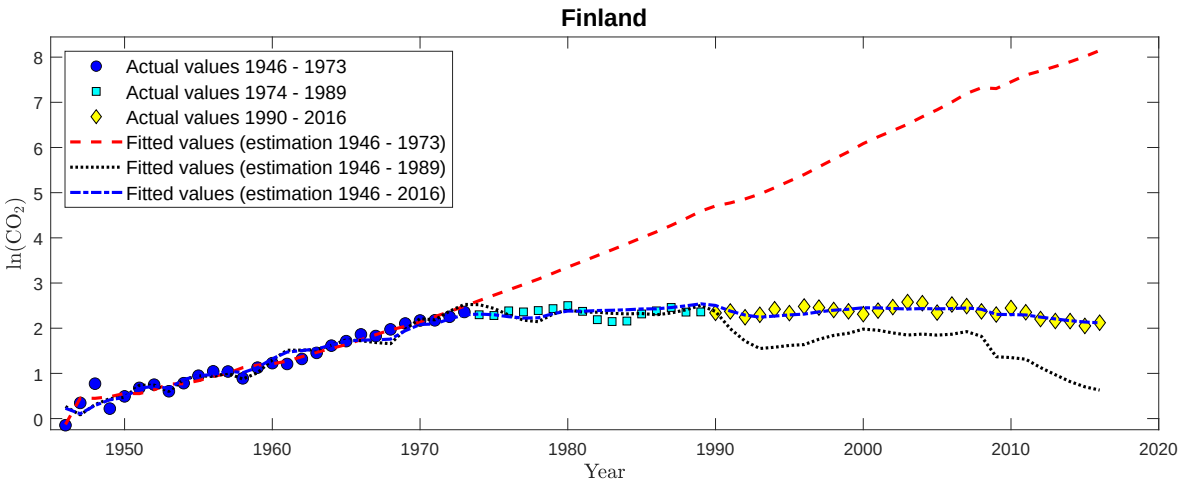

Figure 27: IM-OLS estimation results for a cointegrating quadratic relationship between log per capita GDP and log per capita CO_2 emissions for Finland. The figure shows pairs of observations of log per capita GDP and log per capita CO_2 emissions, for 1946–1973 (blue circles), 1974–1989 (turquoise squares) and 1990–2016 (yellow diamonds). The lines display fitted values over time obtained using different samples for parameter estimation: the dashed red line 1946–1973, the dotted black line 1946–1989 and the dash-dotted blue 1946–2016.

	1946–2016		
	θ_{D_1}	θ_{X_1}	θ_{X_2}
	Australia		
FM-OLS	0.004	**16.542**	**-0.786**
IM-OLS	0.007	**15.218**	**-0.729**
	Belgium		
FM-OLS	**-0.022**	3.355	-0.125
IM-OLS	**-0.017**	*4.869*	-0.213
	Canada		
FM-OLS	**-0.029**	0.624	0.056
IM-OLS	**-0.027**	2.256	-0.030
	Denmark		
FM-OLS	**-0.053**	**8.091**	*-0.265*
IM-OLS	**-0.051**	**8.548**	*-0.291*
	Finland		
FM-OLS	**-0.032**	**13.660**	**-0.593**
IM-OLS	**-0.029**	**15.157**	**-0.674**
	Italy		
FM-OLS	**-0.022**	**5.892**	**-0.207**
IM-OLS	**-0.014**	**11.367**	**-0.500**

	1946–2016		
	θ_{D_1}	θ_{X_1}	θ_{X_2}
	Japan		
FM-OLS	*-0.009*	**3.323**	**-0.123**
IM-OLS	-0.004	**5.070**	**-0.222**
	Portugal		
FM-OLS	**-0.021**	**-3.283**	**0.272**
IM-OLS	**-0.025**	**-4.487**	**0.343**
	Spain		
FM-OLS	**-0.034**	1.488	0.019
IM-OLS	**-0.036**	1.856	0.003
	Sweden		
FM-OLS	**-0.052**	**14.870**	**-0.621**
IM-OLS	**-0.066**	**10.487**	*-0.373*
	United Kingdom		
FM-OLS	**-0.032**	**9.229**	**-0.399**
IM-OLS	**-0.033**	**7.205**	**-0.295**
	United States		
FM-OLS	**-0.030**	**5.733**	**-0.204**
IM-OLS	**-0.023**	**8.414**	**-0.350**

Table 16: FM-OLS and IM-OLS estimation results for a cointegrating quadratic relationship between log per capita GDP and log per capita CO_2 emissions for the full sample period 1946–2016. *Italic* entries indicate significance of coefficients at the 10% level and **bold** entries significance of coefficients at the 5% level.

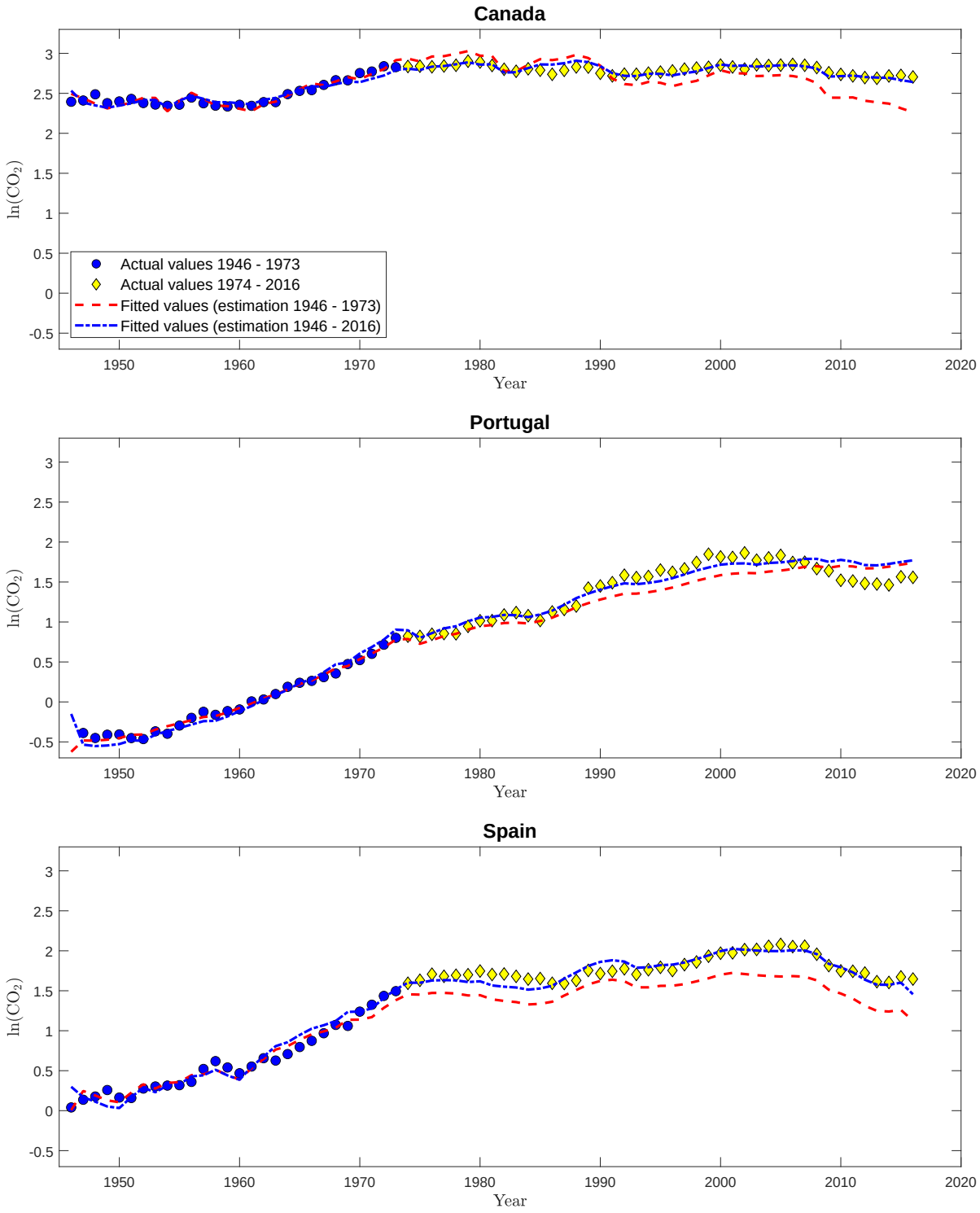

Figure 28: IM-OLS estimation results for a cointegrating linear relationship between log per capita GDP and log per capita CO_2 emissions for Canada, Portugal and Spain. For further explanations see notes to Figure 8 in the main document.

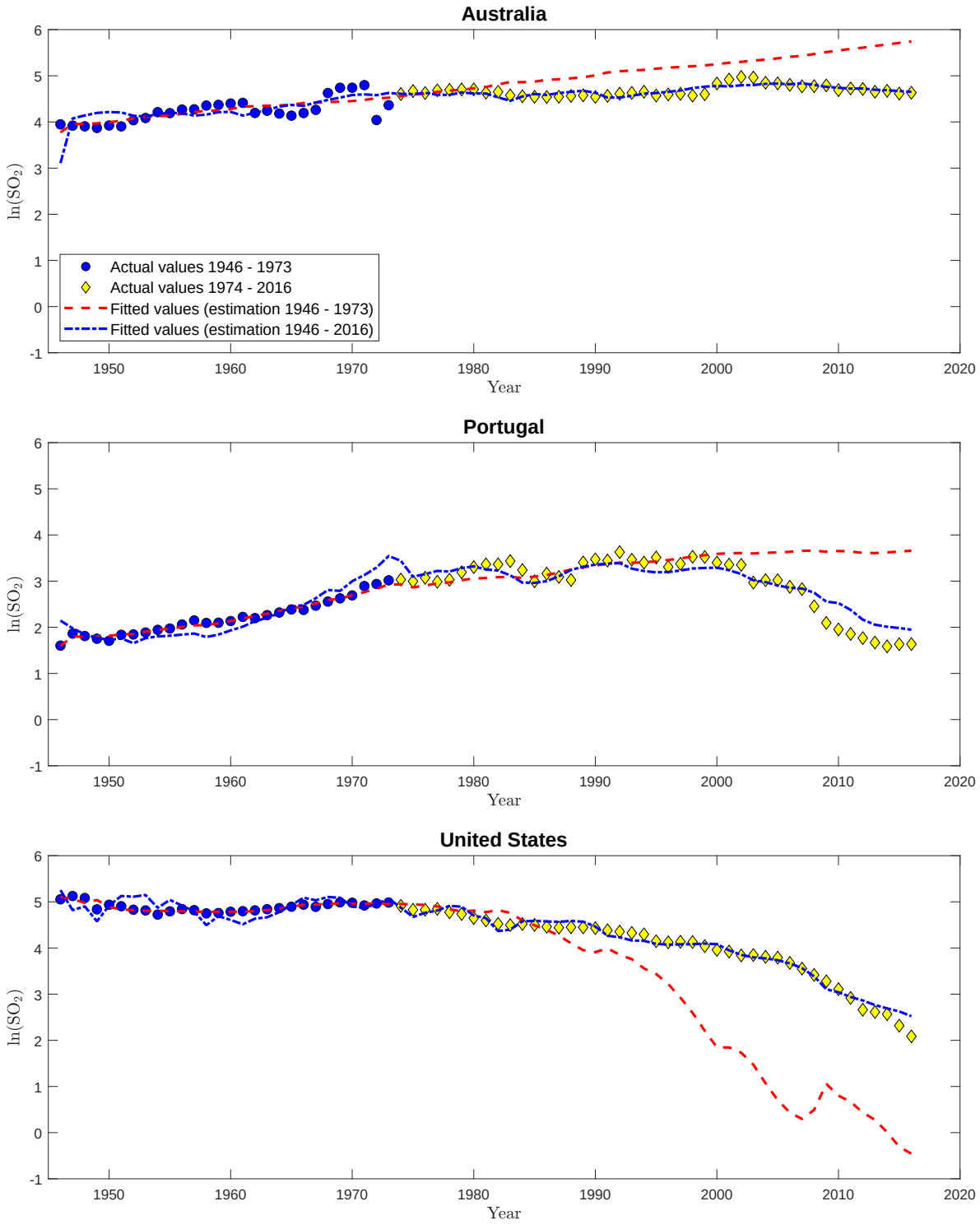

Figure 29: IM-OLS estimation results for a cointegrating linear relationship between log per capita GDP and log per capita SO_2 emissions for Australia and Portugal, and a cointegrating cubic relationship for the United States. For further explanations see notes to Figure 9 in the main document.

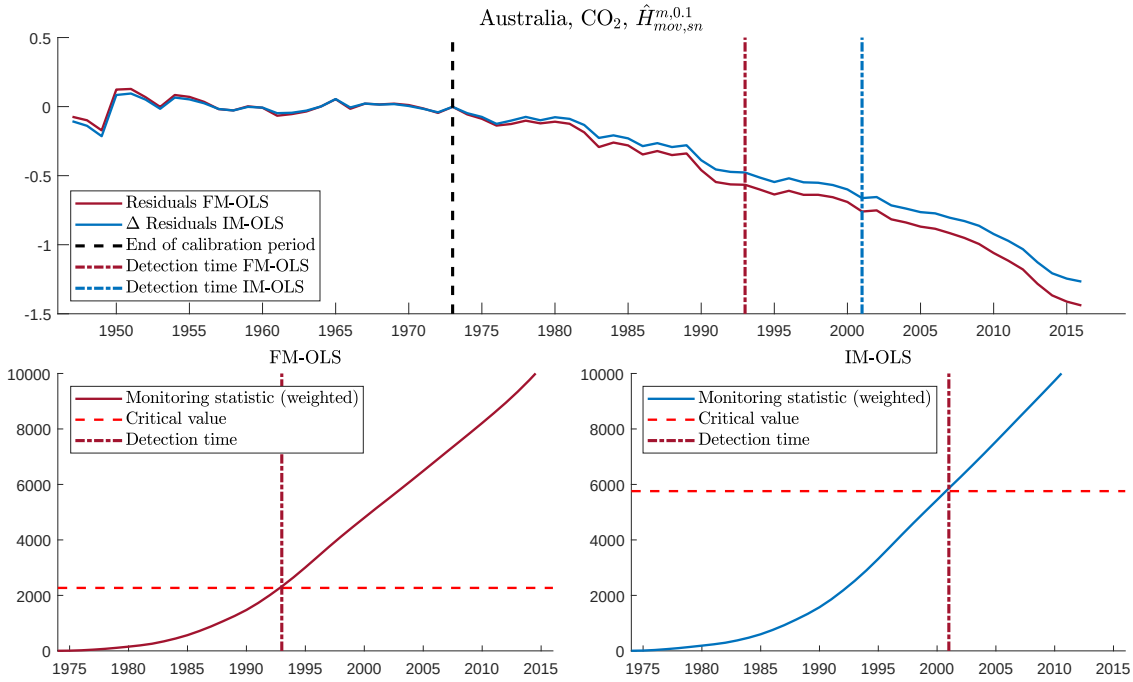

Figure 30: Monitoring results for CO_2 emissions of Australia using $\hat{H}^{m,0.1}_{mov,sn}$ with both, FM-OLS and IM-OLS, in the linear specification. The lower panel shows the detectors, the critical values and the detection times for FM-OLS on the left hand side and for IM-OLS on the right hand side.

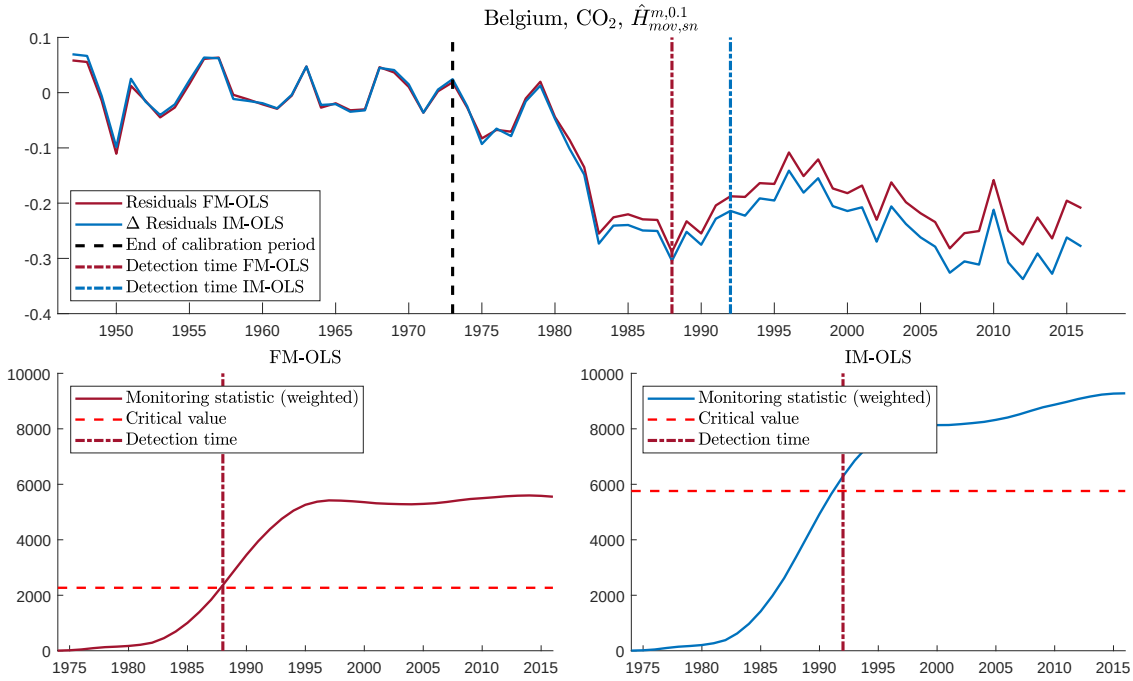

Figure 31: Monitoring results for CO_2 emissions of Belgium using $\hat{H}^{m,0.1}_{mov,sn}$ with both, FM-OLS and IM-OLS, in the linear specification. For further explanations see notes to Figure 30.

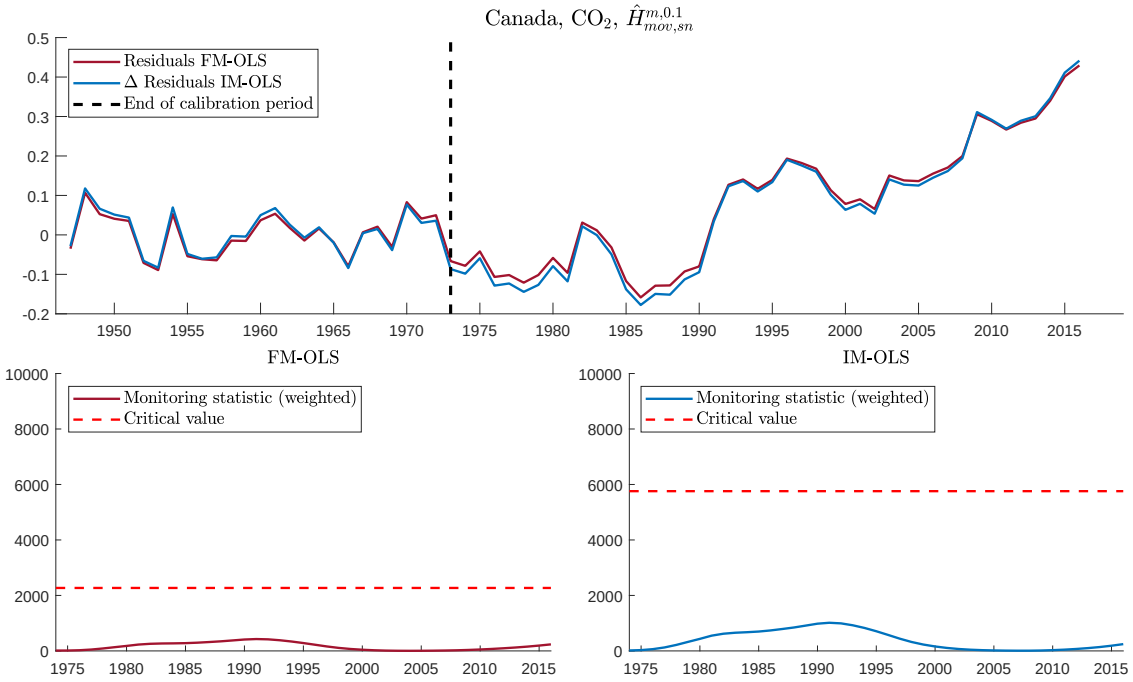

Figure 32: Monitoring results for CO_2 emissions of Canada using $\hat{H}^{m,0.1}_{mov,sn}$ with both, FM-OLS and IM-OLS, in the linear specification. For further explanations see notes to Figure 30.

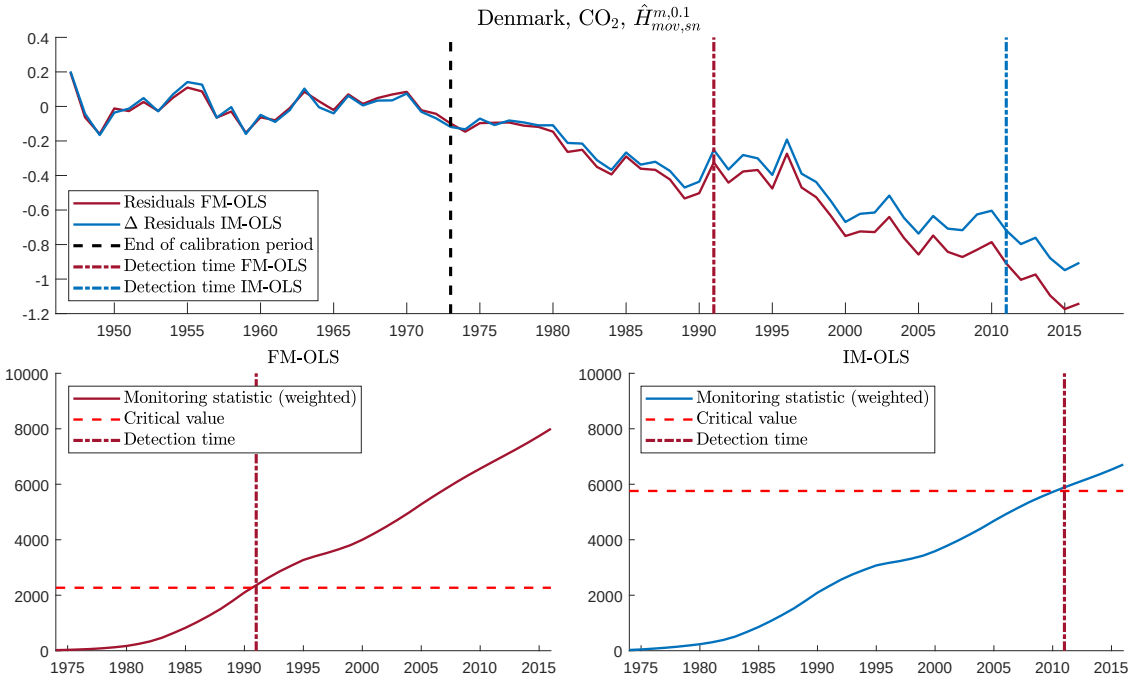

Figure 33: Monitoring results for CO_2 emissions of Denmark using $\hat{H}^{m,0.1}_{mov,sn}$ with both, FM-OLS and IM-OLS, in the linear specification. For further explanations see notes to Figure 30.

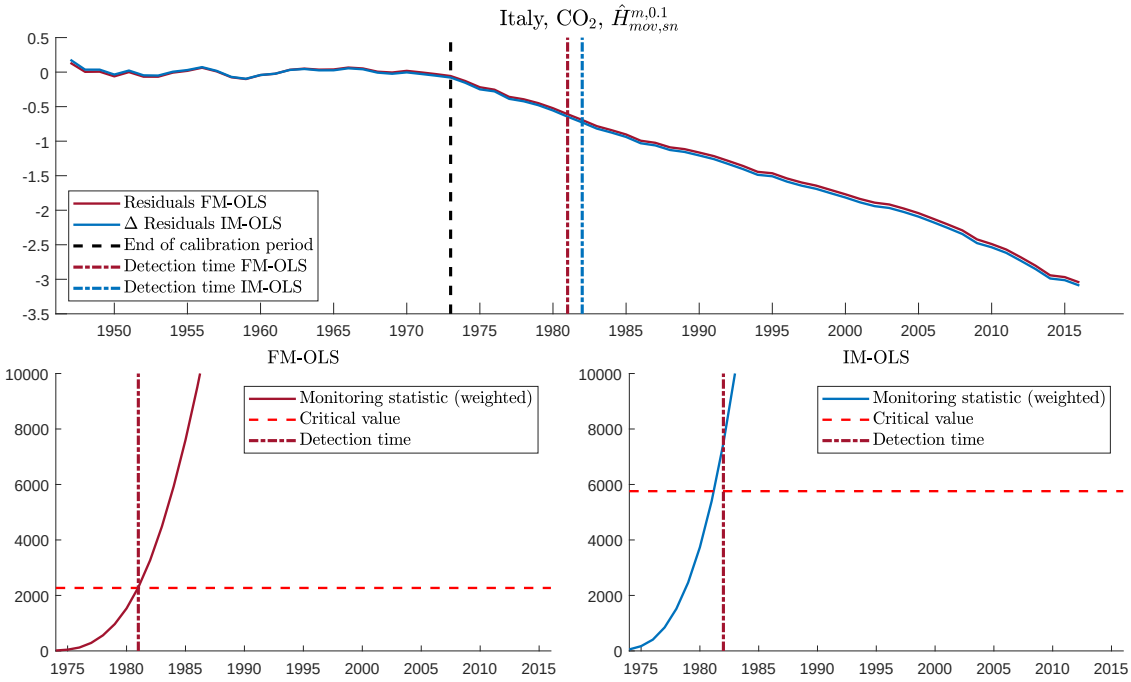

Figure 34: Monitoring results for CO_2 emissions of Italy using $\hat{H}^{m,0.1}_{mov,sn}$ with both, FM-OLS and IM-OLS, in the linear specification. For further explanations see notes to Figure 30.

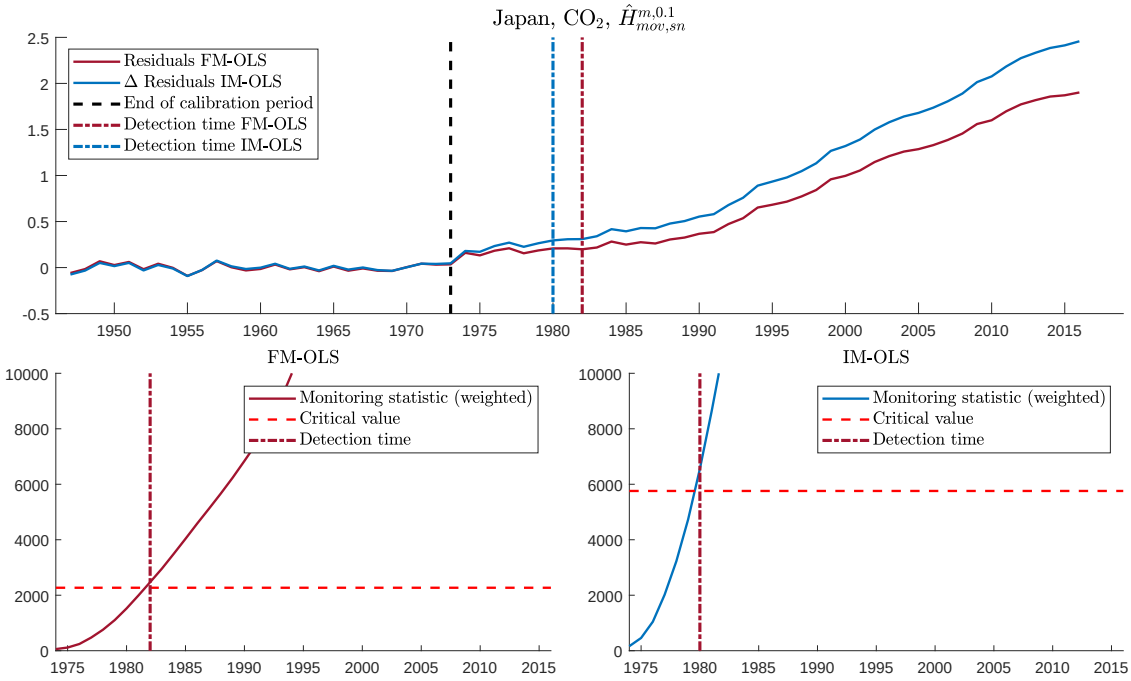

Figure 35: Monitoring results for CO_2 emissions of Japan using $\hat{H}^{m,0.1}_{mov,sn}$ with both, FM-OLS and IM-OLS, in the linear specification. For further explanations see notes to Figure 30.

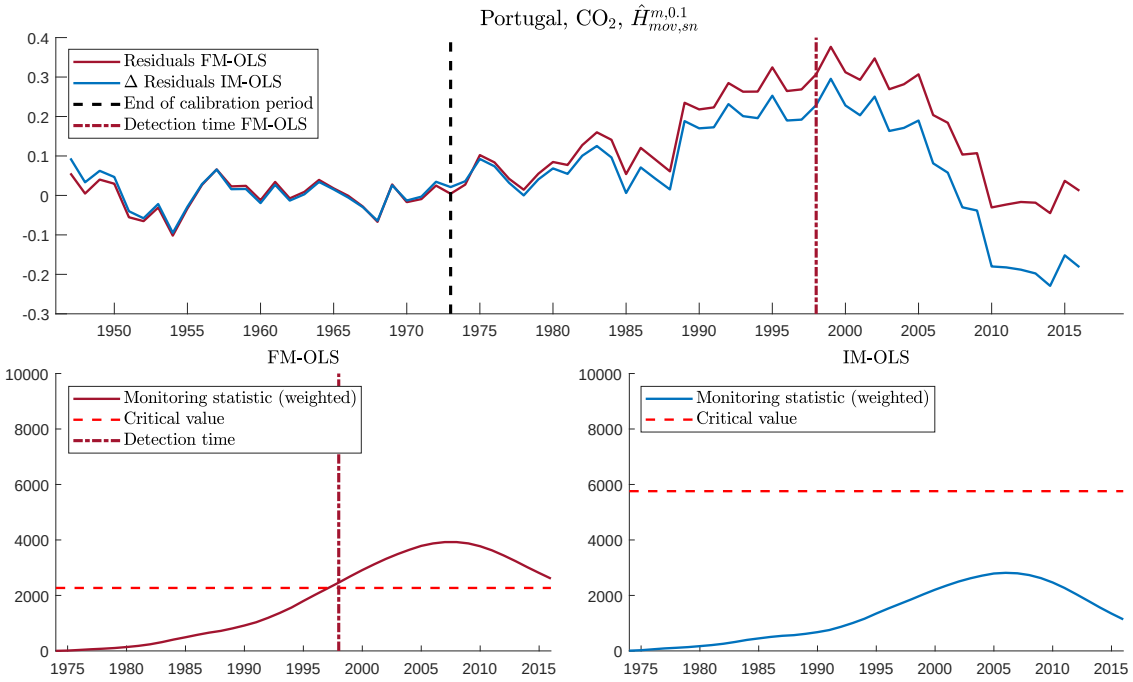

Figure 36: Monitoring results for CO_2 emissions of Portugal using $\hat{H}^{m,0.1}_{mov,sn}$ with both, FM-OLS and IM-OLS, in the linear specification. For further explanations see notes to Figure 30.

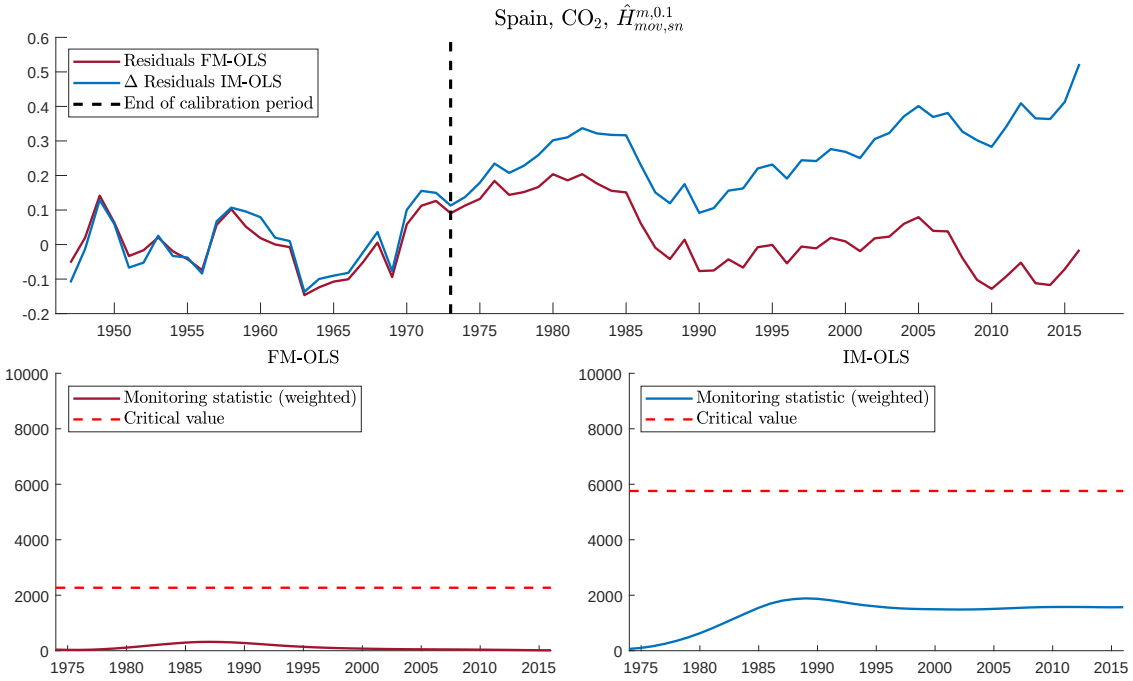

Figure 37: Monitoring results for CO_2 emissions of Spain using $\hat{H}^{m,0.1}_{mov,sn}$ with both, FM-OLS and IM-OLS, in the linear specification. For further explanations see notes to Figure 30.

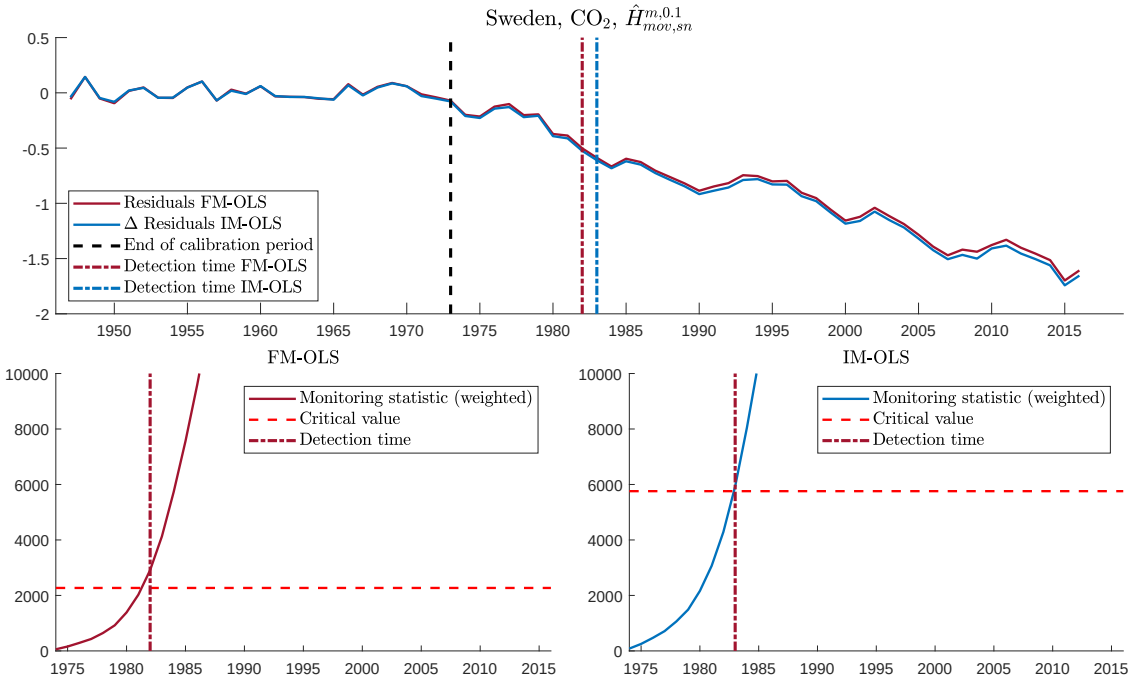

Figure 38: Monitoring results for CO_2 emissions of Sweden using $\hat{H}^{m,0.1}_{mov,sn}$ with both, FM-OLS and IM-OLS, in the linear specification. For further explanations see notes to Figure 30.

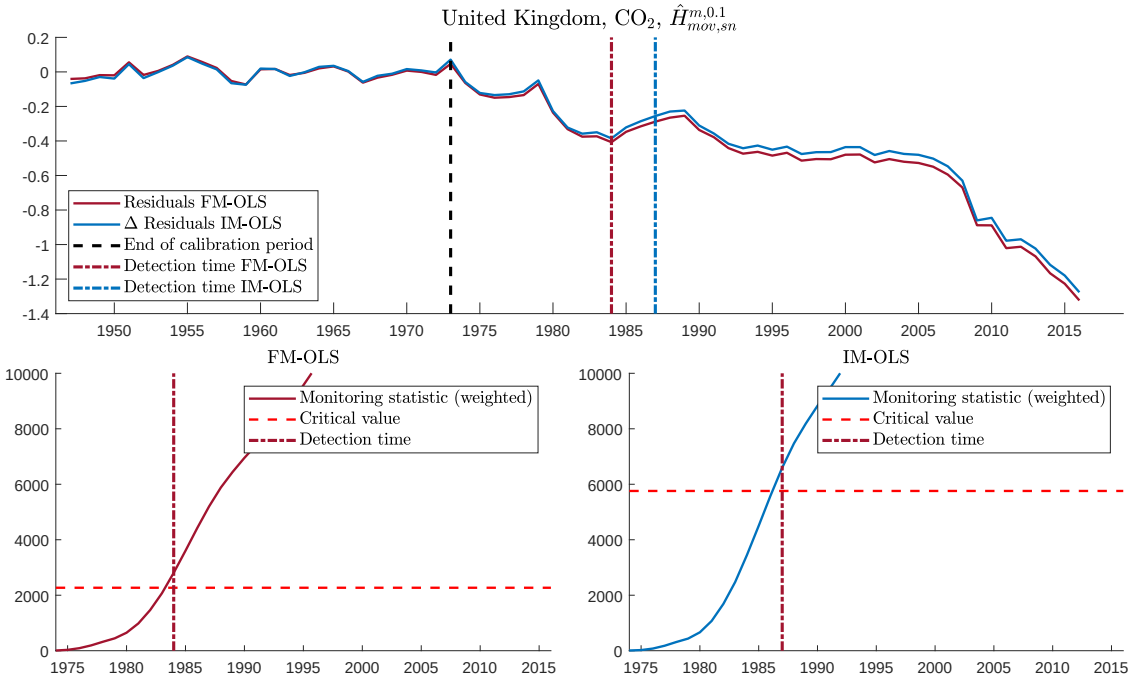

Figure 39: Monitoring results for CO_2 emissions of the United Kingdom using $\hat{H}^{m,0.1}_{mov,sn}$ with both, FM-OLS and IM-OLS, in the linear specification. For further explanations see notes to Figure 30.

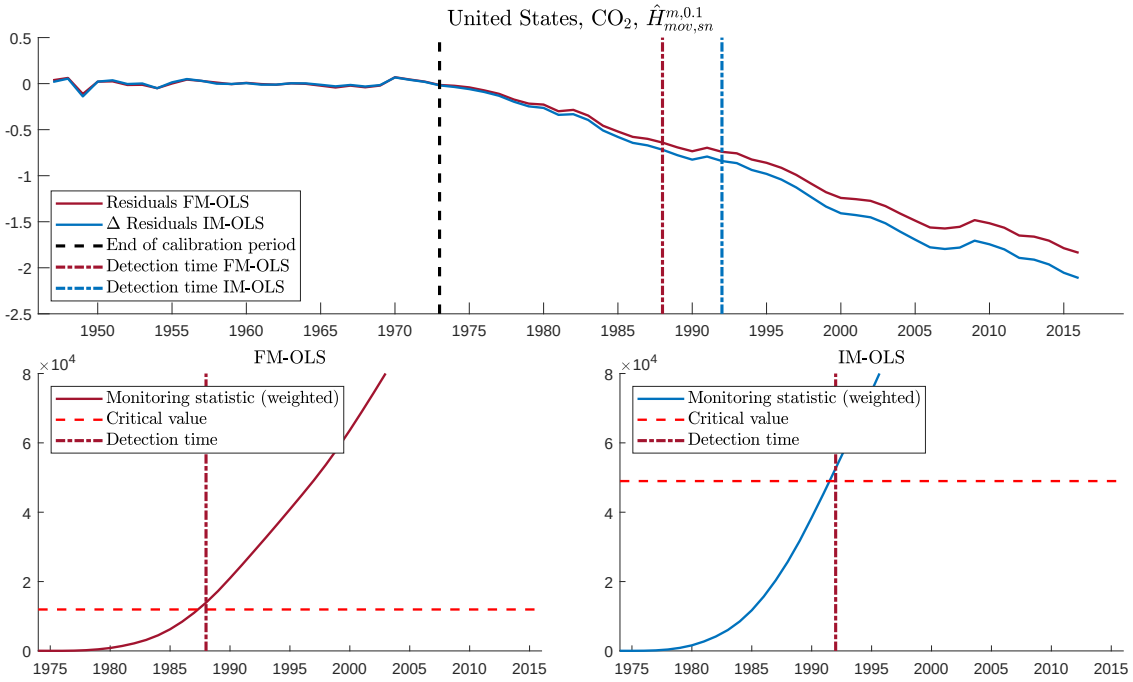

Figure 40: Monitoring results for CO_2 emissions of the United States using $\hat{H}^{m,0.1}_{mov,sn}$ with both, FM-OLS and IM-OLS, in the quadratic specification. For further explanations see notes to Figure 30.

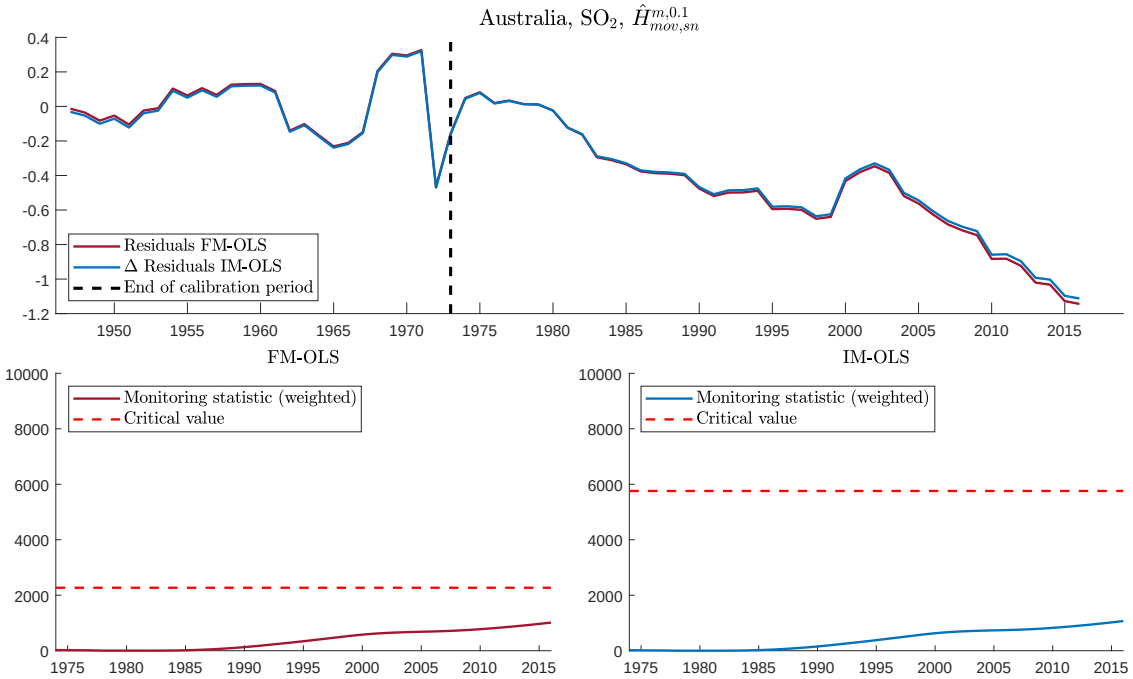

Figure 41: Monitoring results for SO_2 emissions of Australia using $\hat{H}^{m,0.1}_{mov,sn}$ with both, FM-OLS and IM-OLS, in the linear specification. For further explanations see notes to Figure 30.

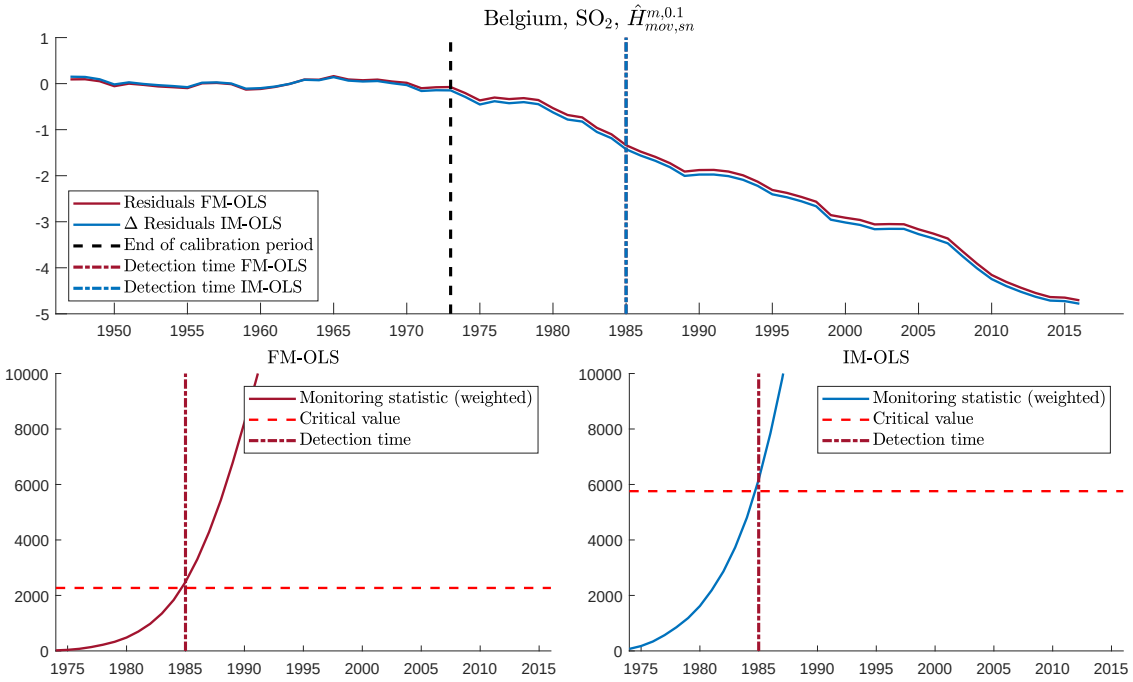

Figure 42: Monitoring results for SO_2 emissions of Belgium using $\hat{H}^{m,0.1}_{mov,sn}$ with both, FM-OLS and IM-OLS, in the linear specification. For further explanations see notes to Figure 30.

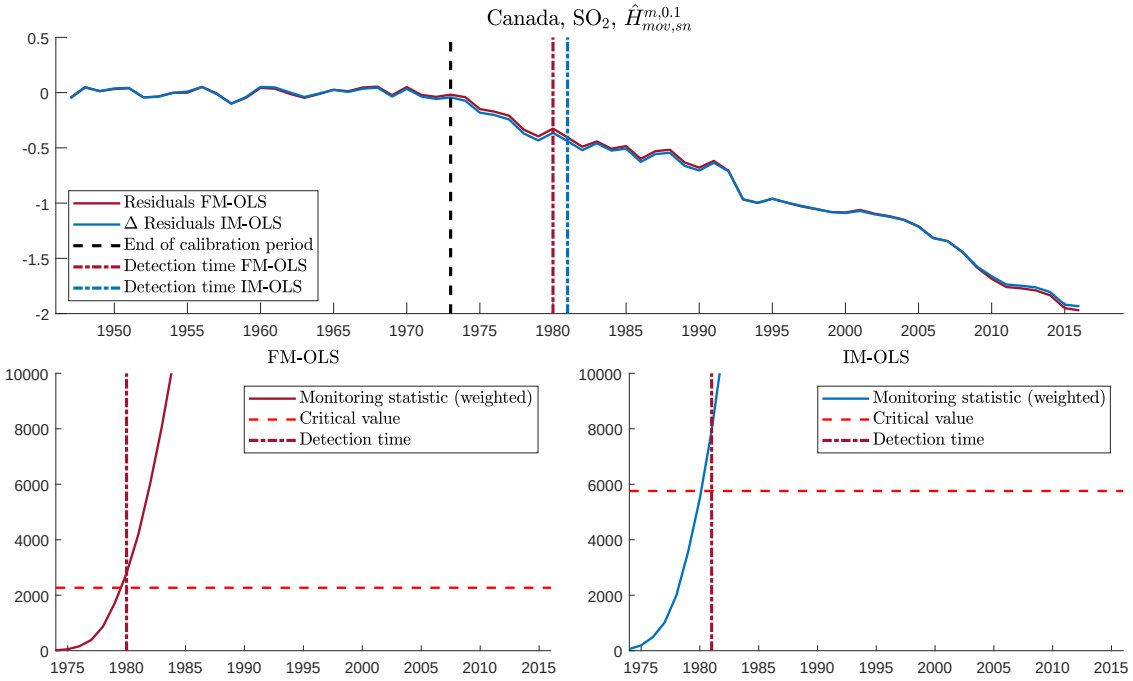

Figure 43: Monitoring results for SO_2 emissions of Canada using $\hat{H}^{m,0.1}_{mov,sn}$ with both, FM-OLS and IM-OLS, in the linear specification. For further explanations see notes to Figure 30.

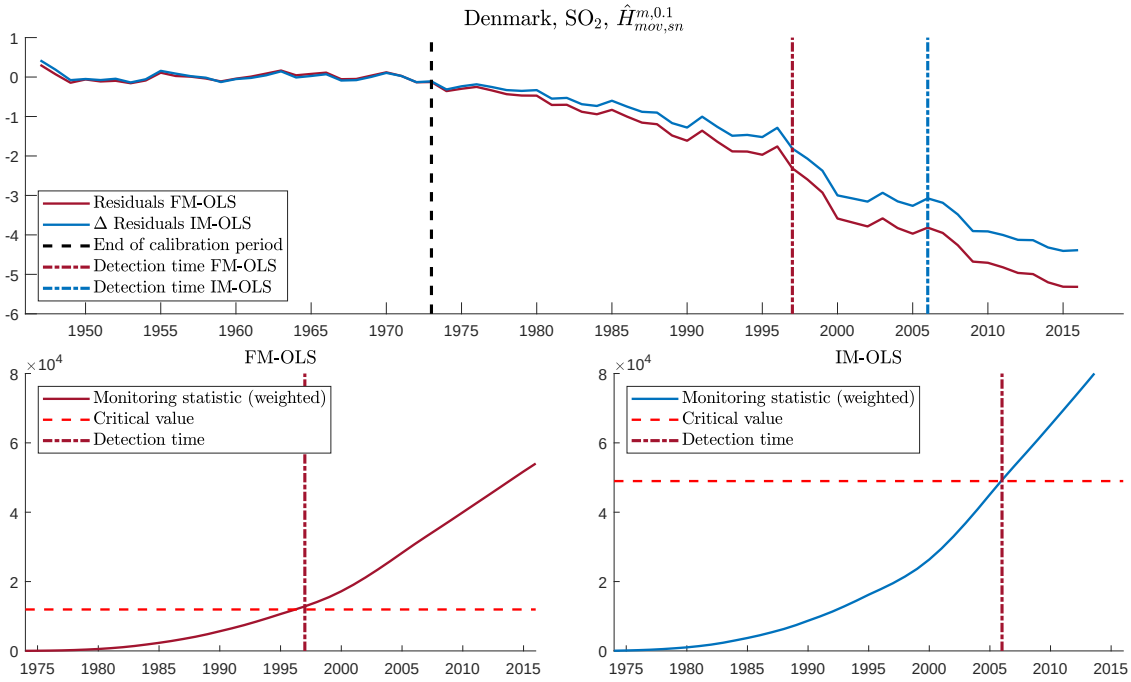

Figure 44: Monitoring results for SO_2 emissions of Denmark using $\hat{H}^{m,0.1}_{mov,sn}$ with both, FM-OLS and IM-OLS, in the quadratic specification. For further explanations see notes to Figure 30.

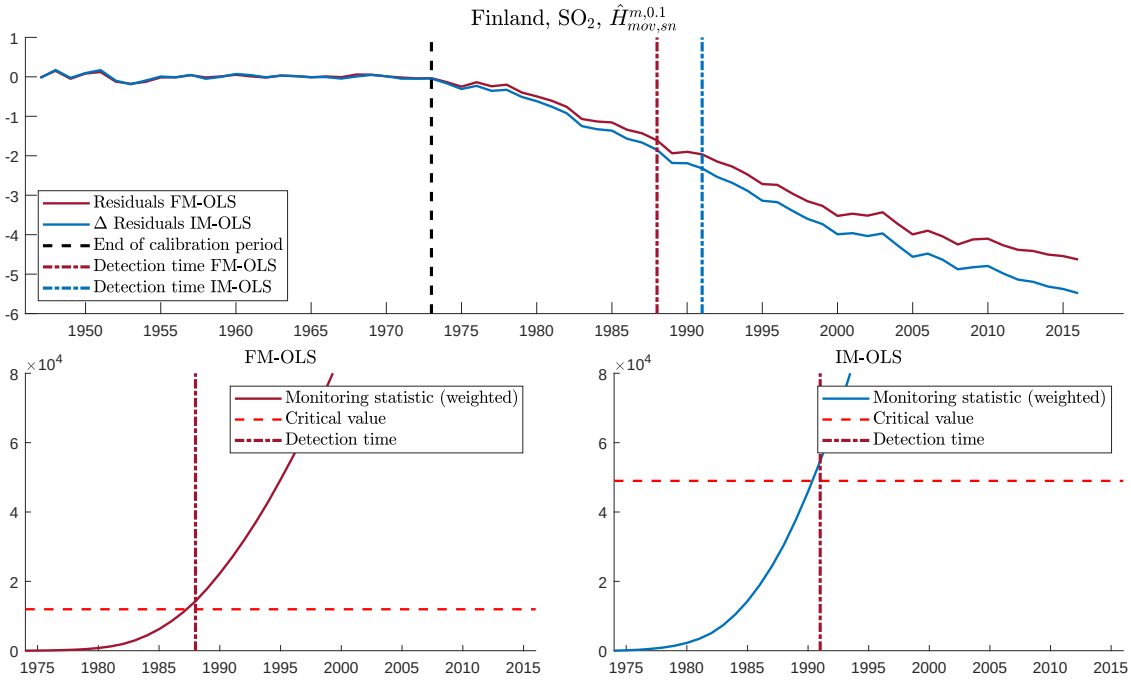

Figure 45: Monitoring results for SO_2 emissions of Finland using $\hat{H}^{m,0.1}_{mov,sn}$ with both, FM-OLS and IM-OLS, in the quadratic specification. For further explanations see notes to Figure 30.

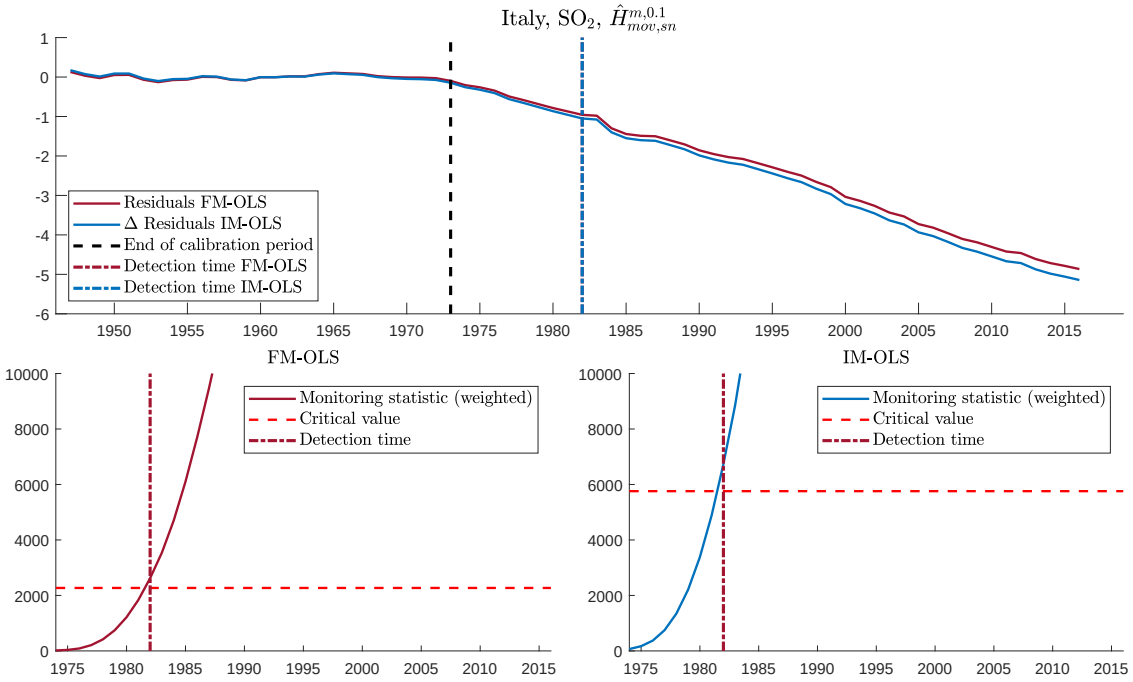

Figure 46: Monitoring results for SO_2 emissions of Italy using $\hat{H}^{m,0.1}_{mov,sn}$ with both, FM-OLS and IM-OLS, in the linear specification. For further explanations see notes to Figure 30.

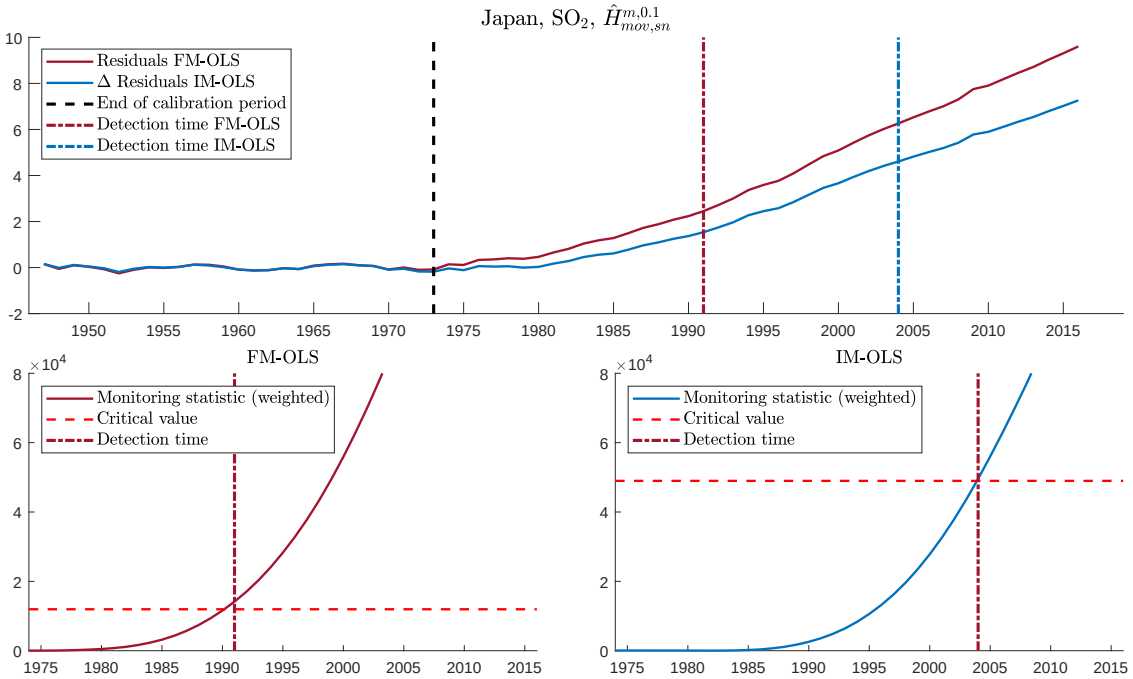

Figure 47: Monitoring results for SO_2 emissions of Japan using $\hat{H}^{m,0.1}_{mov,sn}$ with both, FM-OLS and IM-OLS, in the quadratic specification. For further explanations see notes to Figure 30.

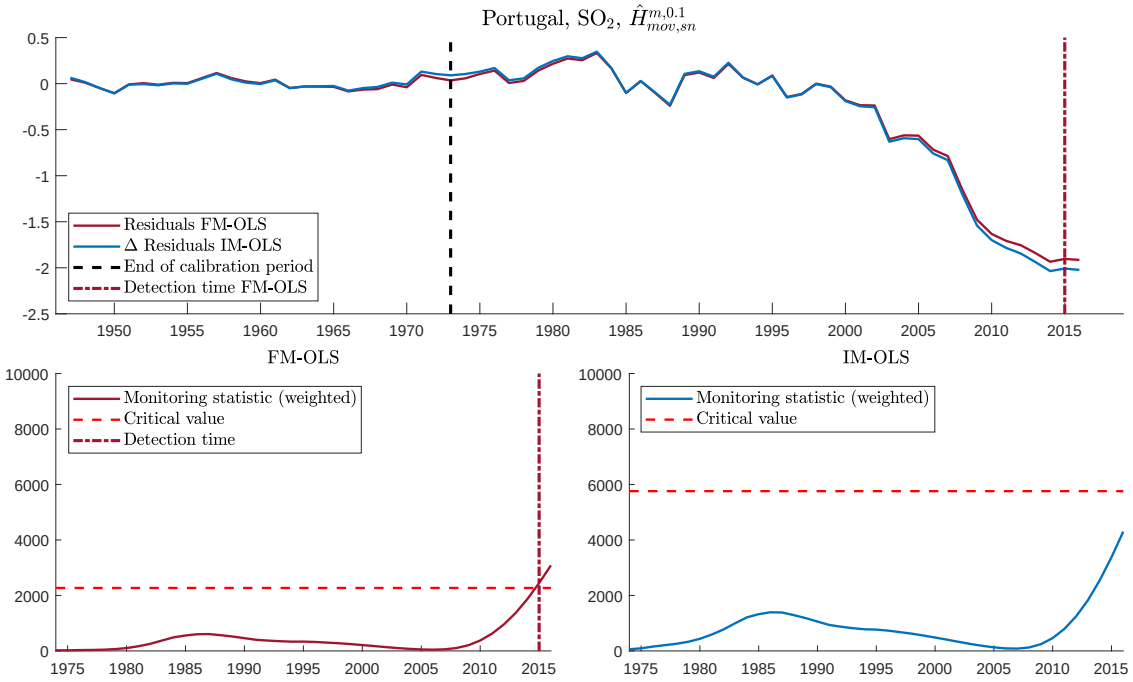

Figure 48: Monitoring results for SO_2 emissions of Portugal using $\hat{H}^{m,0.1}_{mov,sn}$ with both, FM-OLS and IM-OLS, in the linear specification. For further explanations see notes to Figure 30.

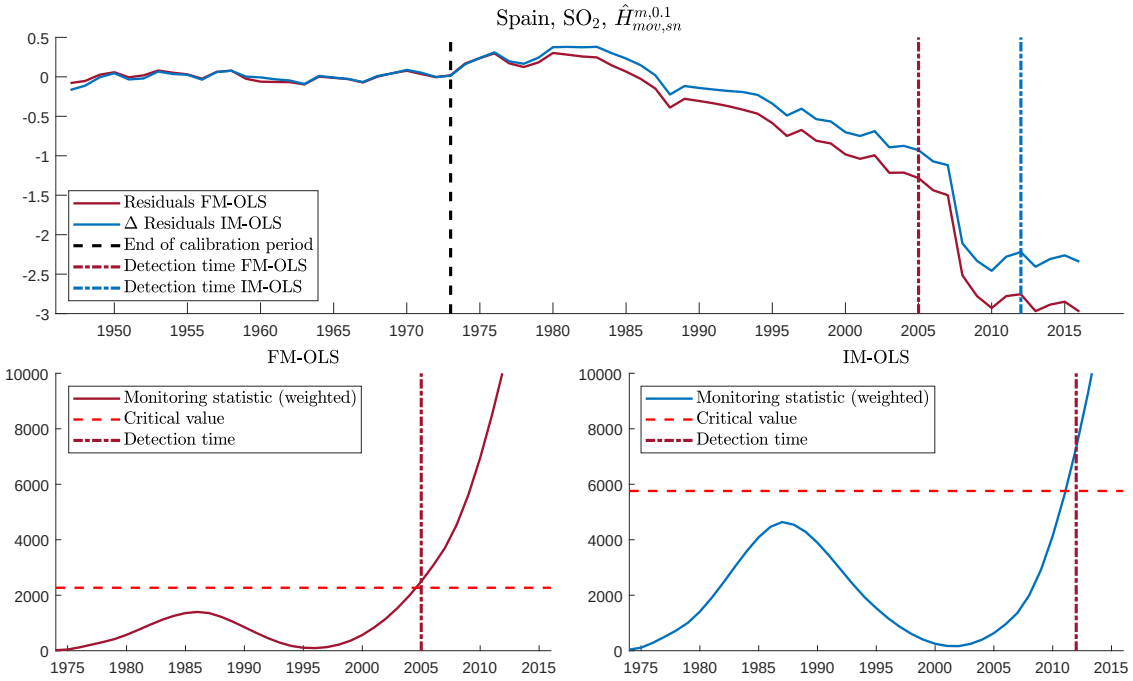

Figure 49: Monitoring results for SO_2 emissions of Spain using $\hat{H}^{m,0.1}_{mov,sn}$ with both, FM-OLS and IM-OLS, in the linear specification. For further explanations see notes to Figure 30.

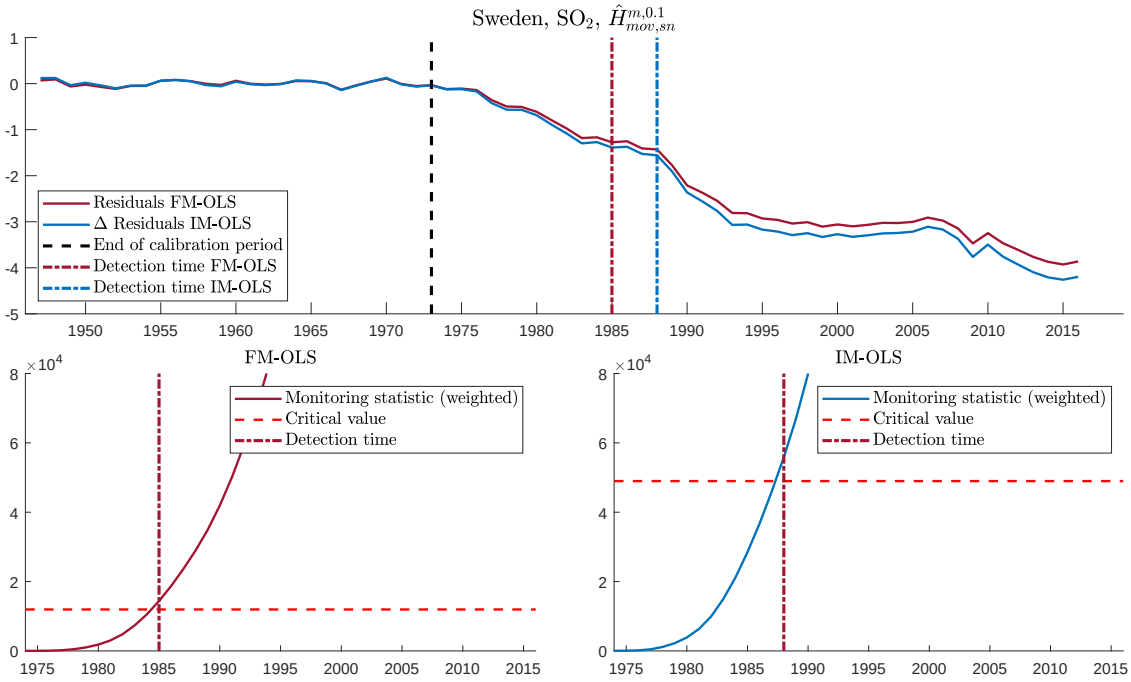

Figure 50: Monitoring results for SO_2 emissions of Sweden using $\hat{H}^{m,0.1}_{mov,sn}$ with both, FM-OLS and IM-OLS, in the quadratic specification. For further explanations see notes to Figure 30.

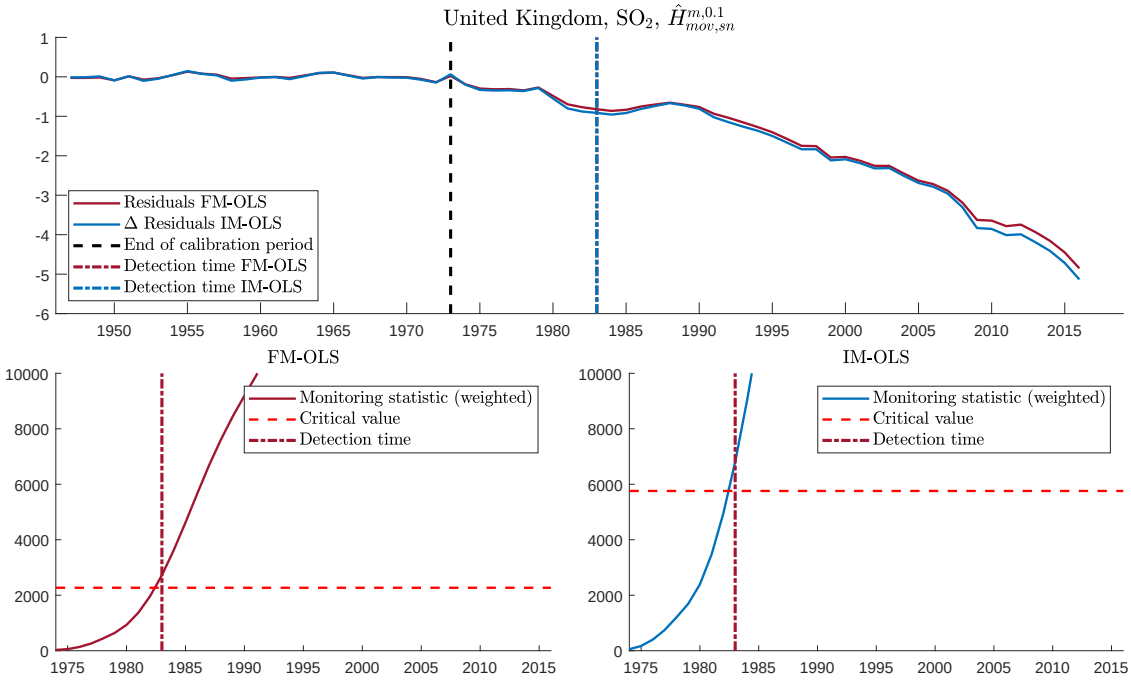

Figure 51: Monitoring results for SO_2 emissions of the United Kingdom using $\hat{H}^{m,0.1}_{mov,sn}$ with both, FM-OLS and IM-OLS, in the linear specification. For further explanations see notes to Figure 30.

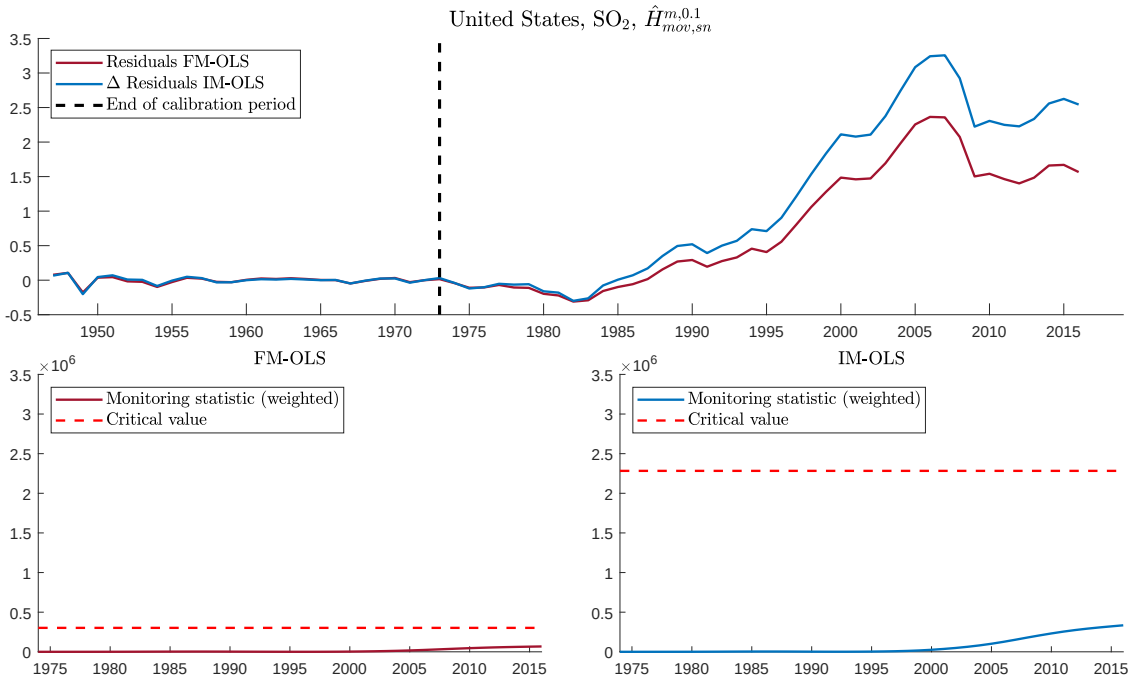

Figure 52: Monitoring results for SO_2 emissions of the United States using $\hat{H}^{m,0.1}_{mov,sn}$ with both, FM-OLS and IM-OLS, in the cubic specification. For further explanations see notes to Figure 30.

References

Dickey, D.A. and W.A. Fuller (1981). Likelihood Ratio Statistics for Autoregressive Time Series with a Unit Root. *Econometrica* **49**, 1057–1072.

Johansen, S. (1995). *Likelihood-based Inference in Cointegrated Vector Autoregressive Models.* Oxford University Press, Oxford.

Phillips, P.C.B. and P. Perron (1988). Testing for a Unit Root in Time Series Regression. *Biometrika* **75**, 335–346.

Shin, Y. (1994). A Residual Based Test for the Null of Cointegration Against the Alternative of No Cointegration. *Econometric Theory* **10**, 91–115.

Vogelsang, T.J. and M. Wagner (2014a). Integrated Modified OLS Estimation and Fixed-b Inference for Cointegrating Regressions. *Journal of Econometrics* **178**, 741–760.

Wagner, M. (2020). Residual Based Cointegration and Non-Cointegration Tests for Cointegrating Polynomial Regressions. Revised and resubmitted to *Empirical Economics*.

Wagner, M. and D. Wied (2017). Consistent Monitoring of Cointegrating Relationships: The US Housing Market and the Subprime Crisis. *Journal of Time Series Analysis* **38**, 960–980.